Palaeogeography, Palaeoclimatology, Palaeoecology 500 (2018) 69–83

Contents lists available at ScienceDirect

Palaeogeography, Palaeoclimatology, Palaeoecology

journal homepage: www.elsevier.com/locate/palaeo

Carbonate REE + Y signatures from the restricted early marine phase of South Atlantic Ocean (late Aptian – Albian): The influence of early anoxic diagenesis on shale-normalized REE + Y patterns of ancient carbonate rocks

Sergio Caetano-Filho[a,*], Gustavo M. Paula-Santos[b], Dimas Dias-Brito[c]

[a] Instituto de Geociências, Universidade de São Paulo, São Paulo, SP 05508-080, Brazil
[b] Instituto de Geociências, Universidade Estadual de Campinas, Campinas, SP 13083-870, Brazil
[c] Centro de Geociências Aplicadas ao Petróleo – UNESPetro, Universidade Estadual Paulista, Rio Claro, SP 13506-900, Brazil

ARTICLE INFO

Keywords:
Rare earth elements
Paleoceanography
Paleoenvironments
Campos Basin
Redox proxies

ABSTRACT

Rare earth elements plus yttrium have been extensively applied in paleoenvironmental studies of ancient carbonate successions due to their fractionation in the marine environment. However, in modern marine anoxic environments, seawater REE + Y signatures can be suppressed in reducing conditions (e.g. stagnant basins and/or early diagenesis) by REE remobilization from several sedimentary components (e.g. detrital siliciclastics, oxides, organic compounds). We present the shale-normalized REE + Y signatures for a transgressive marine carbonate succession of the primitive South Atlantic Ocean (latest Aptian-Albian), in a restricted marine setting with anoxic bottom conditions, to provide and evaluate the REE + Y record deposited in such conditions. Based on well-constrained paleoenvironmental reconstruction through microfacies analysis, three shale normalized REE + Y patterns were identified, varying according to the microfacies associations (MA) and related diagenetic environments: a) light REE-enriched patterns in the more proximal MA associated with burial diagenesis at the base of section; b) flat patterns towards distal MA related to anoxic and sulfidic early diagenesis; and c) middle REE-enriched patterns in MA related to dissolution of Fe—Mn oxy-hydroxide grains under reducing early diagenesis. Cerium anomalies are absent due to stagnant water mass conditions, in accordance with previous studies for the early marine South Atlantic. Y/Ho ratios are lower than modern seawater values, with an increasing trend towards more distal facies. The "non-seawater" shale-normalized REE + Y patterns of the marine carbonates from the primitive South Atlantic Ocean corroborate studies in modern marine reducing environments, in which REE can be remobilized from detrital phases, oxides and organic compounds, suppressing the primary seawater REE + Y signature of authigenic minerals. Caution is suggested for the sole use of carbonate REE + Y signatures as paleoenvironmental proxies, especially in ancient successions lacking proper microfaciological components.

1. Introduction

Rare earth elements plus yttrium (REE + Y) have been extensively used in marine geochemistry and paleoenvironmental studies due to their particular fractionation and cycling on the marine setting. Although they represent an homogeneous group concerning chemical behavior, the progressive filling of the 4f electron shell with increasing atomic number (lanthanide contraction) leads to changes in the chemical properties of these elements in the seawater (e.g. Alibo and Nozaki, 1999; Bertram and Elderfield, 1993; De Baar et al., 1985, 1988; Elderfield and Greaves, 1982; German et al., 1995; Nozaki, 2001; Piper and Bau, 2013; Zhang and Nozaki, 1996, 1998). REE + Y data from seawater and marine sediments are normalized for standard shale concentrations (e.g. Post-Archean Australian Shale – PAAS; McLennan, 1989) to represent the marine REE + Y fractionation processes in relation to the average upper crust composition, as the main source of REE + Y to the ocean are eolian and fluvial influxes (Lawrence et al., 2006; Zhang and Nozaki, 1996, 1998).

REE are trivalent cations in seawater, with the exception of Ce in oxygenated conditions, and their fractionation occurs due to differences in the stability constants of the formed REE-complexes (mainly carbonates, e.g. Cantrell and Byrne, 1987; Johannesson and Lyons, 1994). Increasing atomic number leads to more stable complexation in seawater resulting in more effective removal of light REE (LREE) relatively

* Corresponding author.
E-mail addresses: sergio.caetano.filho@usp.br (S. Caetano-Filho), gustavomps@ige.unicamp.br (G.M. Paula-Santos), dimasdb@rc.unesp.br (D. Dias-Brito).

https://doi.org/10.1016/j.palaeo.2018.03.028
Received 9 October 2017; Received in revised form 6 March 2018; Accepted 25 March 2018
Available online 29 March 2018
0031-0182/

to heavy REE (HREE) by adsorptive scavenging onto surface coatings of the particulate matter (Fe—Mn oxy-hydroxides and organic matter; Sholkovitz et al., 1994). Therefore, a striking feature of shale-normalized REE + Y patterns of seawater is an enrichment of HREE over LREE. Other remarkable features in REE + Y patterns are the positive La anomaly and the pronounced negative Ce anomaly (Alibo and Nozaki, 1999; Bertram and Elderfield, 1993; De Baar et al., 1985; Elderfield and Greaves, 1982; Nozaki, 2001; Piper and Bau, 2013; Zhang and Nozaki, 1996, 1998). Due to empty 4f electron shell, lanthanum is an exception among LREE forming more stable complexes in seawater and kept in solution, which results in positive La anomalies.

In oxygenated seawater column, Ce^{3+} is rapidly oxidized to Ce^{4+}, forming insoluble complexes which are preferentially adsorbed onto particulate coatings (especially Fe—Mn oxides and hydroxides; De Baar et al., 1988; Nozaki et al., 1997; Piper, 1974a; Zhang and Nozaki, 1996), a process mediated by biological activity (Moffett, 1990). Hence, Ce has a redox fractionation not observed in other REE and negative Ce anomalies are commonly found in the modern ocean (e.g. Alibo and Nozaki, 1999; De Baar et al., 1988; Elderfield and Greaves, 1982). This process occurs mainly in the upper water column, with the negative Ce anomaly increasing with depth given the oxidizing reaction and scavenging through deeper water (Tachikawa et al., 1999). Another trace element of interest in marine geochemistry is yttrium, which has chemical behavior similar to HREE and ionic radii closer to Ho. However, Ho is scavenged two times faster than Y by the particulate matter (Nozaki et al., 1997). This results in superchondritic Y/Ho ratios of seawater, much greater than the upper crust ratios (seawater Y/Ho > 60; Bau et al., 1995; Nozaki et al., 1997; Zhang et al., 1994; average upper crust Y/Ho ~26; Kamber et al., 2005).

Given the remarkable REE + Y fractionation and signatures present in seawater, several studies have applied shale-normalized REE + Y data as paleoenvironmental/paleoceanographic proxies through the past decades, especially in carbonate sediments, which would record REE + Y patterns of coeval seawater (e.g. Bau and Dulski, 1996; Bolhar and Van Kranendonk, 2007; Delpomdor et al., 2013; Frimmel, 2009; Nothdurft et al., 2004; Webb and Kamber, 2000; Zhao and Jones, 2013; Zhao et al., 2009). Shale-normalized REE + Y patterns of ancient carbonate rocks have been used to distinguish marine vs. non-marine environments or near-shore vs. open marine conditions (Bolhar and Van Kranendonk, 2007; Frimmel, 2009; Nothdurft et al., 2004; Wang et al., 2014; Webb and Kamber, 2000) through comparison between carbonates and modern seawater patterns, as well as La anomaly and Y/Ho ratios. The Ce anomaly is used as redox proxy for reconstructing oxic vs. suboxic-anoxic conditions of ancient marine environments (e.g. Bolhar and Van Kranendonk, 2007; Jiedong et al., 1999; Ling et al., 2013; Liu and Schmitt, 1984; Liu et al., 1988; Wang et al., 1986).

However, anoxic bottom waters and early anoxic diagenesis can recycle REE scavenged onto particulate matter, attenuating the "seawater" pattern (HREE enrichment) to more flat patterns, due to dissolution of Fe—Mn oxy-hydroxides coatings and destabilization of REE complexes, resulting in REE release, as well as Ce reduction and inversion of negative Ce anomalies to absent or even positive ones (De Baar et al., 1988; Elderfield and Sholkovitz, 1987; German and Elderfield, 1989, 1990; Haley et al., 2004; Kim et al., 2012; Schijf et al., 1991). These processes can affect the REE + Y signatures of authigenic minerals, overcoming the overlying seawater signature (German and Elderfield, 1989, 1990).

Here, we present REE + Y data for carbonate rocks from the initial marine stage of the South Atlantic Ocean (late Aptian-Albian). At this time, the paleogeography reconstructed for the South Atlantic resembles a paratethyan tropical gulf (Fig. 1A; Arai, 2014; Azevedo, 2004; Dias-Brito, 2000), limited by São Paulo – Walvis Ridge at the south, with restricted circulation patterns and anoxic bottom waters (Bolli et al., 1978; Caetano-Filho et al., 2017; Hart and Koutsoukos, 2015; Koutsoukos et al., 1991; Ryan and Cita, 1977). This study aims to provide the shale-normalized REE + Y compositions for the early marine carbonates of South Atlantic Ocean, from proximal to more distal facies of the platform, and discuss the possible influence of restricted circulation patterns and anoxic bottom conditions over REE + Y signals of ancient carbonate rocks. Such effect is important to understand and interpret REE + Y data from carbonate successions lacking the proper paleoenvironmental proxies (e.g. microfossils).

2. Geological setting

2.1. The southeastern Brazilian continental margin and the early marine carbonate deposition in South Atlantic Ocean

The southeastern Brazilian continental margin extends from the Santos Basin (in the south) to the Espírito Santo Basin (in the north) and, as well as other South Atlantic basins, is linked to the Gondwana breakup and the subsequent South Atlantic Ocean opening, initiated in Late Jurassic. This area is inserted in the general model for a passive margin evolution, divided into three tectono-stratigraphic phases (Chang and Kowsmann, 1987; Ojeda, 1982; Ponte and Asmus, 2004): (i) continental rift (clastic deposits; Late Jurassic – Early Cretaceous); (ii) transitional SAG (lacustrine carbonates and evaporites; Aptian); and (iii) drift phase, which was initiated in a context of a restricted carbonate marine environment during the Aptian – mid Albian, to open marine-oceanic conditions from the latest Albian (Dias-Brito and Azevedo, 1986).

In the Campos Basin (Fig. 1B), the referred tectono-stratigraphic phases above are represented by three 2nd-order sequences (Winter et al., 2007): (i) the "Rift Supersequence", with flood basalts (Cabiúnas Formation – Hauterivian), clastic (Itabapoana and Atafona formations – Barremian) and lacustrine bioclastic carbonate deposits (Coqueiros Formation – Early Aptian); (ii) the "Post-Rift Supersequence" (Aptian), represented by lacustrine shales and microbial limestones (Gargaú and Macabu formations) overlapped by evaporites (Retiro Formation); and (iii) the "Drift Supersequence", which comprises the following two depositional sequences, related to the oceanic development of the South Atlantic. The first marine sequence is represented by the Macaé Group, encompassing the mentioned Aptian – mid Albian restricted marine carbonate platform deposits (Quissamã and Outeiro formations), the pelagic late Albian carbonate sediments of Outeiro Formation, which represent the drowning of the previous platform, and the organic-rich shales of the Imbetiba Formation (Cenomanian). The second depositional sequence comprises progradational-retrogradational stacking patterns from the Turonian to Recent, represented by proximal deposits, shales and marlstones, with local occurrences of bioclastic carbonate rocks (Campos Group).

The studied section is composed of carbonates rocks and shales from Quissamã and Outeiro formations, base of the Macaé Group (Figs. 1C and 2), representing the earliest marine environments of South Atlantic Ocean in the SE Brazilian margin. The Quissamã Formation encompasses oolitic to oncolitic grainstones and packstones accumulated in high to moderate energy environments of an internal carbonate ramp (Esteves et al., 1987; Guardado et al., 1989). The pelagic sediments of the Outeiro Formation are represented by wackestones, mudstones, and shales bearing planktonic foraminifera, pithonellids, and radiolarians (Dias-Brito, 1987). On the uppermost part of the Macaé Group, marlstones and organic-rich shales of the Imbetiba Formation point to the end of Cretaceous carbonate deposition, which was caused by significant tectonic and climatic changes in the basin (Dias-Brito and Azevedo, 1986; Spadini et al., 1988).

The pre-latest Albian Quissamã and Outeiro sediments are associated with the "pre-oceanic phase" of Dias-Brito and Azevedo (1986), and record an inefficient connection with coeval oceans within a context of restricted circulation pattern (Azevedo, 2004). At this time, the South Atlantic was an arm of the Tethys Sea, more properly a paratethyan tropical gulf, lacking coral and rudistid reefs, as well as large foraminifera such as orbitolinids, discyclinids and alveolinids in

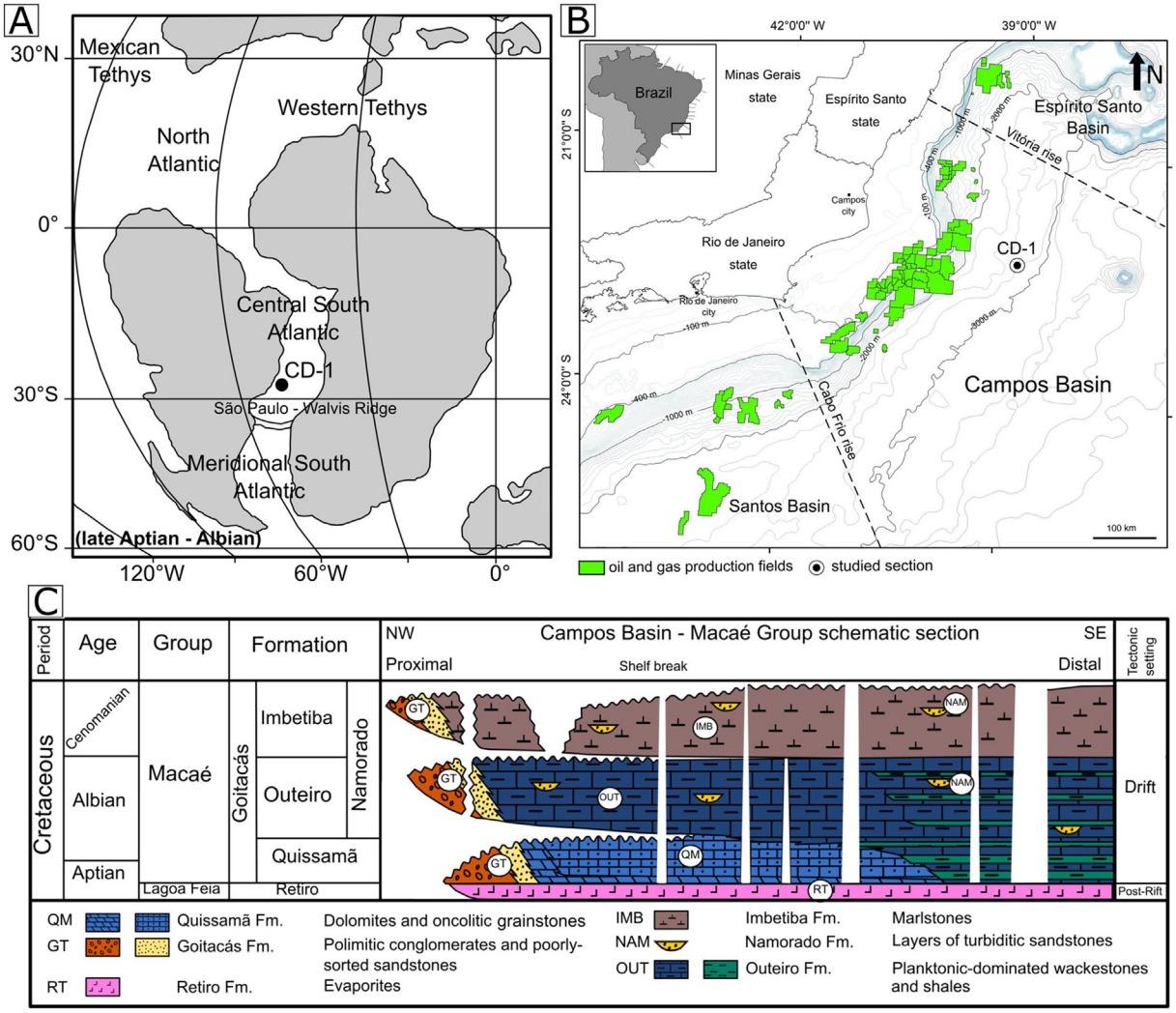

Fig. 1. A) Paleogeography reconstruction for the primitive South Atlantic Ocean during Aptian – Albian (modified from Sabatino et al., 2015). The central South Atlantic was limited by São Paulo-Walvis Ridge in the south (e.g. Azevedo, 2004). CD-1: studied section; B) Location map of studied section in Campos Basin, SE Brazilian continental margin; C) Stratigraphic chart of Macaé Group, Campos Basin (after Winter et al., 2007).

shallow areas. Instead, these areas were dominated by oncolites with low biotic diversity, even in interbank areas, in a scenario of a hypersaline neritic environment, under warm and dry weather conditions. Nevertheless, a very strong Tethyan influence is noticed on the distal deposits, represented by the pelagic microbiota, including the termophilic pithonellids, collomielids (calpionellids), favusellids, nannoconids, stemless crinoids (e.g., roveacrinids), as observed, for example, in Mexico and Gulf of Mexico (Carvalho et al., 1999; Dias-Brito, 1994, 1995, 2000). The São Paulo-Walvis Ridge was a barrier to open circulation on the south (Fig. 1A).

2.2. Studied section

The CD-1 section corresponds to the base of an exploration well, drilled in a distal part of the Campos Basin (SE Brazilian continental margin), under ~2850 m water depth and overlain by > 5000 m of marine deposits (from 5340 to 5652 mbsf). A transgressive succession is registered, controlled by well-constrained paleoenvironmental reconstruction based on microfacies analysis, in which an anoxic organic-preservation event is present (Caetano-Filho et al., 2017; Fig. 2). Three informal units were divided, from the base to the top (Fig. 2): (i) Unit I (5650 to 5620 m deep), composed of mudstones, bioclastic wackestones, and packstones with benthic-dominated faunas, associated with the Quissamã Formation, which overlies evaporites of the Retiro Formation; (ii) Unit II (5620 to 5570 m deep), as an allochthonous evaporite (anhydrite) layer in distal compressive regime of the margin (e.g. Mohriak, 2004, 2009); and (iii) Unit III (5570 to 5335 m deep) composed of frequent intercalations of bioclastic wackestones, mudstones, and shales with a planktonic-dominated biota and increased TOC contents, which was associated with the Outeiro Formation.

The detailed microfaciological analysis and chemostratigraphy of the CD-1 section was presented by Caetano-Filho et al. (2017). Five carbonate microfacies association (MA) were identified and disposed in a carbonate ramp model (e.g. Guardado et al., 1989). MA-1 records an interbank environment of low-energy and well-oxygenated conditions located in an inner ramp, and the limestones are composed of bioclastic wackestones with miliolids and articulated ostracodes in a free-terrigenous micritic matrix. MA-2 was associated with a flank of a carbonate bank, in moderated-energy and well-oxygenated environment, encompassing peloidal/bioclastic packstones (miliolids and ostracodes) and wackestones with local terrigenous laminations. MA-3 is related to a middle ramp in a low-energy and well-oxygenated environment; it is composed of bioclastic wackestones with some bioturbation, including agglutinated foraminifers, pelagic microcrinoids, and planktonic foraminifers. This microfacies association has a relatively high TOC content (> 0.5%). MA-4 represents the most distal domain (outer ramp), in a low-energy and oxygen-depleted environment. This is suggested by the association of three elements: (a) predominance of planktonic

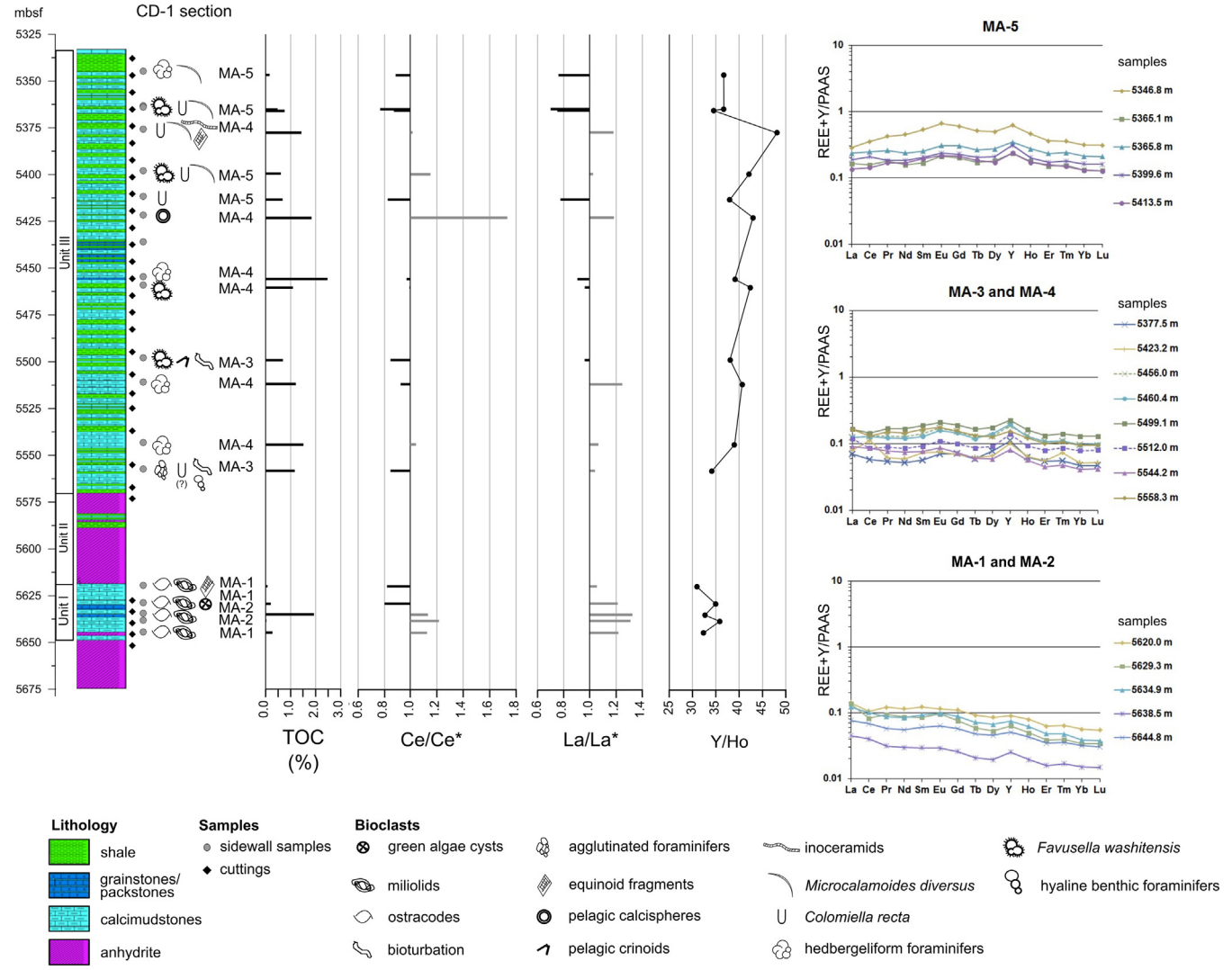

Fig. 2. The CD-1 section, divided in three informal units (I–III), lithological column, samples, and microfossil content along the studied interval, accompanied by Total Organic Carbon, Ce anomaly, La anomaly, and Y/Ho profiles. On the right, the REE + Y/PAAS spider diagrams from the carbonates of CD-1 section, grouped by microfacies associations.

organisms, including *Favusella washitensis*, *Colomiella recta*, and abundant nannofossils in the matrix; (b) lack of benthic organisms; (c) high TOC content (1.1 to 2.5%). Finally, MA-5 comprises resedimented deposits (tempestites) accumulated in middle to outer ramp, composed of bioclastic wackestones with abundant planktonic organisms (foraminifers, planktonic crinoids, and collomielids) and high terrigenous content. The matrix exhibit a co-occurrence of glauconite grains, Fe—Mn oxides, and framboidal pyrite, pointing to different environmental redox conditions due to sedimentary reworking from shallower and well-oxygenated deposits and transport to deeper environments with oxygen-depleted bottom conditions.

Regarding age constraints for CD-1 section, the studied interval was assigned to the latest late Aptian to early Albian, based on the occurrence of the colomiellid *Colomiella recta* and the rapid increase in $^{87}Sr/^{86}Sr$ ratios, from 0.7072 to 0.7074 (Caetano-Filho et al., 2017). Several microfaciological and biostratigraphic studies ascribed *C. recta* to the upper Aptian – lower Albian interval (Blanco-Bustamante, 2001; Dias-Brito, 1999; Dias-Brito and Ferré, 2001; González-León et al., 2008; Longoria and Monreal, 2009; Madhavaraju et al., 2013; Michalík et al., 2012; Núñez-Useche et al., 2016; Núñez-Useche and Barragan, 2012; Premoli-Silva and Mcnulty, 1984; Vincent et al., 2010), whereas the $^{87}Sr/^{86}Sr$ radiogenic trend through CD-1 section can be assigned to a similar remarkable feature of the Cretaceous Sr isotope stratigraphy, which is related to an enhanced greenhouse stage and consequently increase in continental weathering during the Aptian – Albian transition (Bodin et al., 2015; Bralower et al., 1997; Jones and Jenkyns, 2001). These major oceanic-climate changes are associated with the ocean anoxic event 1b (OAE 1b, late Aptian – early Albian; Erbacher et al., 1999, 2001, Herrle et al., 2004, 2015; Kennedy et al., 2014; Sabatino et al., 2015) and related organic-rich deposits described worldwide.

3. Materials and methods

A total of 18 carbonate sidewall samples were provided by Petrobras. The samples were powdered in an agate pounder for the geochemical analysis. Major elements, TOC, and insoluble residues were used for data evaluation and discussions, and the related analytical procedures were described by Caetano-Filho et al. (2017).

Trace elements analysis was performed by inductively coupled mass spectrometry (ICP-MS), with particularly interest on the REE + Y concentrations of the carbonate fraction. Before dissolution, the samples were cleaned by reaction with HNO_3 10% for 24 h and then washed with Milli-Q deionized water. About 0.1000 ± 0.0001 g of limestone powders were homogenized with 5 mL of Milli-Q deionized water and

dissolved with 5 mL purified HNO_3 65%. After the reaction ceased, 15 mL of deionized water was added to homogenize the solution, which was heat to 60 °C for an hour, to release residual CO_2. The samples were cooled during 12 h. After cooled, Milli-Q deionized water was added to solution to complete 40.0 ± 0.2 g and then, centrifuged. The leachate was carefully collected and analyzed in a Thermo Scientific iCap quadrupole ICP-MS, at Geoanalítica-USP Facility, University of São Paulo. The reference materials BR, JGb-1, and ML-2 were run and the obtained results matched the expected for the REE + Y contents.

Rare earth elements data were normalized to Post-Archean Australian Shale (PAAS, McLennan, 1989), and La, Ce, and Eu anomalies were calculated through the geometric average, according to Lawrence et al. (2006). The geometric assumption comes from the graphical linear behavior on a log-linear plot and follows the equations:

$$La/La^* = La_n/(Pr_n^3/Nd_n^2) \quad (1)$$

$$Ce/Ce^* = Ce_n/(Pr_n^2/Nd_n) \quad (2)$$

$$Eu/Eu^* = Eu_n/(Sm_n^2 * Tb_n)^{1/3} \quad (3)$$

where REE_n represents the shale-normalized value. Samples which the calculated values ranged between 0.90 and 1.10, were considered devoid of anomalies. Additionally, $(Nd/Yb)_n$, $(Pr/Yb)_n$, $(Pr/Tb)_n$, and $(Tb/Yb)_n$ were calculated as parameters of relatively enrichments in REE + Y/PAAS patterns (e.g. Lawrence et al., 2006). $(Nd/Yb)_n$ and $(Pr/Yb)_n$ represents light/heavy REE ratios (LREE/HREE), whereas $(Pr/Tb)_n$ and $(Tb/Yb)_n$ are indicators of light/middle REE (LREE/MREE) and middle/heavy REE (MREE/HREE), respectively.

4. Results

Trace and major elements, TOC, insoluble residues contents, PAAS-normalized values, and the calculated REE + Y parameters are presented in Tables 1, 2, and 3, respectively, and in Fig. 2. In unit I, MA-1 (n = 3) and MA-2 (n = 2) presented a remarkable enrichment in LREE over both MREE (MA-1 and MA-2 Pr/Tb_n averages of 1.38 and 1.37, respectively; Table 3) and HREE (MA-1 and MA-2 Nd/Yb_n averages of 2.12 and 2.08, respectively; MA-1 and MA-2 Pr/Yb_n averages of 2.26 and 2.17, respectively; Table 3), as a gradual depletion in REE + Y/PAAS values towards heavier REE (Fig. 2). These microfacies associations presented the lowest ΣREE values (Table 1), with averages of 19 and 14 ppm for MA-1 and MA-2, respectively. MA-1 and MA-2 showed La positive anomalies (La/La* averages of 1.16 and 1.32, respectively; Table 3; Fig. 2) and Eu positive anomalies (Eu/Eu* average of 1.14 and 1.13, respectively; Table 3; Fig. 2). Slight negative to positive Ce anomalies were obtained for MA-1 and positive ones were calculated for MA-2 (Ce/Ce* averages of 0.92 and 1.18, respectively; Table 3; Fig. 2). Both cases are distinct of the prominent negative Ce anomalies of modern well-oxygenated seawater column (e.g. Tachikawa et al., 1999). The average Y/Ho ratios are 32.81 and 34.35 for MA-1 and MA-2, respectively (Table 3; Fig. 2).

In unit III, MA-3 (n = 2) and MA-4 (n = 6) REE + Y/PAAS patterns showed no significant fractionations between LREE and MREE (Pr/Tb_n averages of 1.08 and 1.05 ± 0.13for MA-3 and MA-4, respectively; Table 3; Fig. 3) and depletion of HREE relative to LREE and MREE (MA-3 and MA-4 averages, respectively: Nd/Yb_n of 1.41 and 1.29 ± 0.27; Pr/Yb_n of 1.44 and 1.34 ± 0.28; and Tb/Yb_n of 1.33 and 1.27 ± 0.12; Table 3; Fig. 2). La/La* averages for MA-3 and MA-4 point to absence of La anomaly (1.00 and 1.09 ± 0.14, respectively; Table 3; Fig. 2). Slight Eu positive anomalies were also observed in MA-3 and MA-4 (Eu/Eu* averages of 1.15 and 1.21 ± 0.06, respectively; Table 3; Fig. 2). Slight Ce negative anomalies were found for MA-3 (Ce/Ce* average of 0.85; Table 3; Fig. 2) whereas MA-4 presented variable Ce anomalies (Ce/Ce* average of 1.12 ± 0.31; median of 1.01; Table 3; Fig. 2), most of them around 1.00 and a maximum of 1.74 for the carbonates of CD-1 section (Fig. 2). ΣREE average values are 33 and 21 ± 6 ppm for MA-3 and MA-4, respectively (Table 1). Y/Ho average ratios are 36.13, for MA-3, and 42.03 ± 3.41 for MA-4, with the latter microfacies association presenting the highest Y/Ho ratios in the CD-1 section (Table 3; Fig. 2).

The REE + Y/PAAS patterns of MA-5 also presented enrichment of LREE over HREE (Nd/Yb_n and Pr/Yb_n averages of 1.23 ± 0.14 and 1.27 ± 0.10, respectively; Table 3), but the striking feature is the "hat-type" REE + Y/PAAS pattern, regarding pronounced enrichment in MREE over both LREE and HREE (Fig. 2; Pr/Tb_n and Tb/Yb_n averages of 0.94 ± 0.08 and 1.37 ± 0.16, respectively; Table 3). MA-5 presented average slight negative La and Ce anomalies (average La/La* and Ce/Ce* of 0.81 ± 0.13 and 0.90 ± 0.15, respectively; Table 3; Fig. 2), and positive Eu anomalies (average Eu/Eu*of 1.20 ± 0.06; Table 3; Fig. 2). This microfacies association has the highest REE content (average ΣREE of 51 ± 21 ppm; Table 1) and average Y/Ho of 37.59 ± 2.81 (Table 3; Fig. 2).

The overall REE + Y/PAAS patterns of the marine carbonates of CD-1 section do not register the expected signatures for seawater. Instead, they tend to be closer to shale pattern, approaching flat distributions with no distinctive lanthanum and Ce anomalies. Furthermore, CD-1 carbonates presented overall slight depletion in HREE. The Y/Ho ratios (from 31 to 48) are also lower than expected for seawater, closer to upper crustal values (~26, Kamber et al., 2005). Slight positive Eu anomalies were found for all the samples (except for sample at 5620.00 m). High feldspar contents or analytical interferences related to barium oxide were discarded given no correlation between Th vs. Eu/Eu* and Ba vs. Eu/Eu* ($r = 0.11$ and 0.28, p(a) > 0.10, n = 18, respectively, not shown; e.g. Chen et al., 2014; Frimmel, 2009). A possible hydrothermal influence over total REE + Y contents of CD-1 carbonates is also minimized by the relationship between microfacies associations and REE + Y patterns division presented below. In addition, no petrographic evidences of pervasive hydrothermal activity were observed.

5. Discussion

5.1. Diagenetic alteration and analytical contamination vs. primary controls on carbonate shale-normalized REE + Y patterns

The major challenge in using shale-normalized REE + Y compositions of ancient carbonates for paleoenvironmental/paleoceanographic studies is to identify the possible contamination of the REE + Y contents from other sedimentary phases (e.g. oxides, organic compounds, silicates, sulphides) during post-depositional processes (e.g. diagenesis, hydrothermalism) or analytical procedures (acid dissolution). For example, silicates have much higher REE contents compared to carbonates and a minimum exchange of REE between these minerals may overcome the carbonate depositional signature (Nothdurft et al., 2004).

Sc, Th, and Zr are used to track contamination on carbonate REE + Y contents, due to higher amounts of these trace elements in average shale than in marine carbonates (Frimmel, 2009; Nothdurft et al., 2004; Webb and Kamber, 2000). Additionally, Al content from whole-rock geochemistry (Table 1) was used, as representative of terrigenous silicate fraction of the CD-1 carbonates. The diagrams presented in Fig. 3 show moderate to strong positive correlation for Sc vs. ΣREE ($r = 0.76$, p(a) < 0.01, n = 18), Zr vs. ΣREE ($r = 0.42$, p(a) = 0.08, n = 18), Al vs. ΣREE ($r = 0.62$, p(a) < 0.01, n = 18), and Th vs. ΣREE ($r = 0.70$, p(a) < 0.01, n = 18). Although Zr vs. ΣREE correlation is not statistically significant, the positive correlation between Sc, Al, and Th and ΣREE suggests contamination of the REE + Y contents of CD-1 carbonates by terrigenous components. Hence, combined with "non-seawater" type of the CD-1 marine carbonates, the nature of this disturbance in REE + Y/PAAS patterns of the CD-1 marine carbonates must be discussed. Regarding Ce anomalies, we applied some parameters proposed by Shields and Stille (2001) to track post-depositional alterations. Enrichments in total REE (ΣREE) and MREE (decreasing Dy_n/Sm_n ratios), as well as the development of

Table 1
Trace elements, Al, P, insoluble residues, and TOC of the carbonate rocks of CD-1 section.

Depth (mbsf)	MA	Sc (ppm)	Y (ppm)	Zr (ppm)	La (ppm)	Ce (ppm)	Pr (ppm)	Nd (ppm)	Sm (ppm)	Eu (ppm)	Gd (ppm)	Tb (ppm)
5346.8	MA-5	4.8	16.8	0.9	10.9	28.1	3.7	15.3	3.0	0.7	2.8	0.4
5365.1	MA-5	2.8	6.4	1.2	6.2	12.5	1.6	5.3	0.9	0.2	0.9	0.1
5365.8	MA-5	4.2	9.4	1.2	9.0	19.8	2.3	8.0	1.4	0.3	1.4	0.2
5377.5	MA-4	0.8	3.0	0.5	2.7	4.6	0.5	1.8	0.3	0.1	0.3	0.0
5399.6	MA-5	2.9	8.4	0.9	7.2	16.7	1.6	6.2	1.1	0.3	1.1	0.2
5413.5	MA-5	6.0	6.4	1.1	5.2	11.3	1.5	5.7	1.1	0.2	1.0	0.1
5423.2	MA-4	0.6	2.7	1.1	3.0	8.9	0.5	2.0	0.4	0.1	0.3	0.0
5456.0	MA-4	1.9	5.1	1.2	4.7	10.3	1.2	4.4	0.8	0.2	0.7	0.1
5460.4	MA-4	1.4	5.3	1.1	4.8	10.1	1.1	4.1	0.7	0.2	0.7	0.1
5499.1	MA-3	2.7	6.1	2.2	6.3	11.5	1.5	5.6	1.0	0.2	0.9	0.1
5512.0	MA-4	0.8	3.8	1.1	4.6	6.8	0.8	2.9	0.5	0.1	0.5	0.1
5544.2	MA-4	1.1	2.2	0.6	3.5	6.8	0.7	2.5	0.4	0.1	0.3	0.0
5558.3	MA-3	3.1	4.1	1.2	6.3	10.4	1.3	5.0	0.9	0.2	0.7	0.1
5620.0	MA-1	2.1	2.4	0.4	5.5	8.4	1.1	3.9	0.7	0.1	0.5	0.1
5629.3	MA-1	0.9	1.7	0.2	5.2	6.6	0.8	2.9	0.5	0.1	0.4	0.0
5634.9	MA-2	2.2	2.0	0.6	4.7	8.1	0.8	2.9	0.5	0.1	0.4	0.1
5638.5	MA-2	0.2	0.7	0.1	1.7	3.2	0.3	1.0	0.2	0.0	0.1	0.0
5644.8	MA-1	0.9	1.4	0.1	2.9	5.4	0.5	1.9	0.3	0.1	0.3	0.0

Depth (mbsf)	Dy (ppm)	Ho (ppm)	Er (ppm)	Tm (ppm)	Yb (ppm)	Lu (ppm)	Th (ppm)	Ba (ppm)	ΣETR (ppm)	Al (%)	P (%)	Insoluble residue (%)	TOC (%)
5346.8	2.3	0.5	1.0	0.1	0.9	0.1	0.9	79.2	87	1.58	0.06	23.41	0.17
5365.1	0.8	0.2	0.4	0.1	0.4	0.1	0.8	281.4	36	1.25	0.03	17.81	0.50
5365.8	1.3	0.3	0.7	0.1	0.6	0.1	1.0	212.7	55	1.57	0.04	20.56	0.77
5377.5	0.4	0.1	0.2	0.0	0.1	0.0	0.2	61.5	14	0.32	0.02	10.04	1.44
5399.6	1.0	0.2	0.5	0.1	0.5	0.1	0.6	6.5	45	0.97	0.03	13.20	0.61
5413.5	0.8	0.2	0.5	0.1	0.4	0.1	1.2	29.9	34	2.05	0.06	14.74	0.69
5423.2	0.3	0.1	0.2	0.0	0.1	0.0	0.2	41.0	19	0.25	0.02	12.75	1.84
5456.0	0.6	0.1	0.3	0.0	0.3	0.0	0.6	58.3	29	0.83	0.04	18.40	2.49
5460.4	0.7	0.1	0.3	0.0	0.3	0.0	0.3	8.1	28	0.67	0.03	14.98	1.10
5499.1	0.8	0.2	0.4	0.1	0.4	0.1	0.6	155.7	35	0.89	0.03	13.10	0.70
5512.0	0.4	0.1	0.2	0.0	0.2	0.0	0.2	50.2	21	0.27	0.02	6.02	1.22
5544.2	0.3	0.1	0.1	0.0	0.1	0.0	0.3	127.9	17	0.43	0.04	16.00	1.52
5558.3	0.6	0.1	0.3	0.0	0.3	0.0	0.8	128.1	30	1.38	0.02	19.05	1.18
5620.0	0.4	0.1	0.2	0.0	0.2	0.0	0.4	9.9	24	0.68	0.01	9.56	0.09
5629.3	0.2	0.0	0.1	0.0	0.1	0.0	0.2	9.7	19	0.31	0.01	4.37	0.21
5634.9	0.3	0.1	0.1	0.0	0.1	0.0	0.5	53.2	20	1.81	0.04	37.45	1.94
5638.5	0.1	0.0	0.0	0.0	0.0	0.0	0.0	42.0	7	0.08	0.01	1.99	0.04
5644.8	0.2	0.0	0.1	0.0	0.1	0.0	0.1	2.9	13	0.40	0.01	4.38	0.28

Table 2
Shale-normalized REE contents (REE + Y/PAAS) of carbonates from CD-1 section.

Depth (mbsf)	MA	La (PAAS)	Ce (PAAS)	Pr (PAAS)	Nd (PAAS)	Sm (PAAS)	Eu (PAAS)	Gd (PAAS)d	Tb (PAAS)	Dy (PAAS)	Y (PAAS)	Ho (PAAS)	Er (PAAS)	Tm (PAAS)	Yb (PAAS)	Lu (PAAS)
5346.8	MA-5	0.29	0.35	0.42	0.45	0.53	0.66	0.60	0.51	0.50	0.62	0.46	0.36	0.36	0.31	0.31
5365.1	MA-5	0.16	0.16	0.18	0.16	0.17	0.21	0.20	0.17	0.18	0.24	0.18	0.15	0.15	0.13	0.13
5365.8	MA-5	0.24	0.25	0.26	0.24	0.25	0.31	0.30	0.26	0.27	0.35	0.27	0.23	0.24	0.21	0.21
5377.5	MA-4	0.07	0.06	0.05	0.05	0.06	0.07	0.07	0.06	0.08	0.11	0.06	0.05	0.06	0.05	0.05
5399.6	MA-5	0.19	0.21	0.18	0.18	0.21	0.24	0.23	0.20	0.21	0.31	0.20	0.17	0.18	0.16	0.16
5413.5	MA-5	0.14	0.14	0.17	0.17	0.19	0.22	0.21	0.18	0.17	0.24	0.17	0.16	0.15	0.13	0.13
5423.2	MA-4	0.08	0.11	0.06	0.06	0.07	0.08	0.07	0.06	0.07	0.10	0.06	0.06	0.07	0.05	0.05
5456.0	MA-4	0.12	0.13	0.13	0.13	0.14	0.17	0.15	0.13	0.13	0.19	0.13	0.11	0.11	0.10	0.09
5460.4	MA-4	0.13	0.13	0.12	0.12	0.13	0.16	0.15	0.12	0.14	0.20	0.13	0.11	0.11	0.10	0.10
5499.1	MA-3	0.17	0.14	0.17	0.17	0.19	0.21	0.19	0.17	0.18	0.23	0.16	0.13	0.14	0.13	0.13
5512.0	MA-4	0.12	0.09	0.09	0.09	0.09	0.11	0.10	0.09	0.09	0.14	0.09	0.08	0.09	0.08	0.08
5544.2	MA-4	0.09	0.09	0.08	0.07	0.08	0.09	0.07	0.06	0.06	0.08	0.06	0.05	0.05	0.04	0.04
5558.3	MA-3	0.16	0.13	0.15	0.15	0.16	0.17	0.15	0.13	0.13	0.15	0.12	0.10	0.11	0.10	0.09
5620.0	MA-1	0.14	0.11	0.12	0.11	0.12	0.12	0.11	0.09	0.09	0.09	0.08	0.06	0.06	0.06	0.05
5629.3	MA-1	0.14	0.08	0.09	0.09	0.09	0.10	0.08	0.06	0.05	0.06	0.05	0.04	0.04	0.03	0.03
5634.9	MA-2	0.12	0.10	0.09	0.08	0.09	0.10	0.09	0.07	0.07	0.07	0.06	0.05	0.05	0.04	0.04
5638.5	MA-2	0.05	0.04	0.03	0.03	0.03	0.03	0.03	0.02	0.02	0.03	0.02	0.02	0.02	0.02	0.01
5644.8	MA-1	0.08	0.07	0.06	0.06	0.06	0.06	0.06	0.05	0.05	0.05	0.04	0.03	0.04	0.03	0.03

negative Eu anomalies, would follow post-depositional increases in Ce/Ce* (i.e. development of absent or positive Ce anomalies). Fig. 4 shows weak correlation between these parameters, suggesting no post-depositional alteration of Ce/Ce*. The lack of correlation between Ce/Ce* and P also discards influence of authigenic phosphate which can present negative Ce anomaly (Fig. 04; Pattan et al., 2005).

The most important approach is to distinguish whether contamination would have occurred during analytical procedures or post-depositional (hydrothermal or diagenetic) processes. Considering that the HNO_3 acid used in our methodology resulted in an oxidizing reaction, we also have to consider that some REE + Y may have been released from organic compounds into solution during analytical procedures. For this purpose, the relationship between REE + Y/PAAS patterns and microfaciological data provides very important discussions. Although CD-1 carbonates presented a “non-seawater” type, the REE + Y/PAAS patterns vary according to the carbonate microfacies associations described in the studied section (Fig. 02; Caetano-Filho et al., 2017). This is the first and direct observation against contamination during analytical procedures. Microfacies associations were defined primary based on biogenic contents, grains fabric, and depositional texture, in which insoluble residue (e.g. detrital silicates, oxides, sulphides, organic compounds) varies independently from the microfaciological division (Table 1). We also note the lack of correlation between the LREE/HREE index (Nd/Yb_n) and insoluble residue contents ($r = -0.06$, p(a) > 0.10, n = 18), Al content ($r = -0.15$, p(a) > 0.10, n = 18), and TOC ($r = -0.26$, p(a) > 0.10, n = 18; Fig. 5). Here, the LREE/HREE index was chosen as representative of the variability of REE + Y/PAAS patterns in the section, whereas insoluble residue, Al, and TOC contents represent the detrital siliciclastic and organic components. We expect that the increasing contamination degree would lead to higher LREE/HREE, masking the seawater LREE-depleted pattern (e.g. Nothdurft et al., 2004). Therefore, if our analytical procedure leached REE + Y from other phases than carbonates, we would expect a systematic contamination and a direct correlation between LREE/HREE and insoluble residue, Al, and/or TOC contents, which was not observed. We conclude that if the analyzed samples were affected by contamination from other phases than carbonates, it may have occurred during diagenetic processes rather than analytical procedures. Furthermore, considering that the insoluble residue (i.e. detrital and organic compounds) for the three sets of REE + Y/PAAS patterns varies in a closer interval, the straight relationship between them and microfacies associations suggests a paleodepositional control over these signatures, even if the overlying seawater signature would have been suppressed.

The two remaining hypothesis to explain the non-seawater REE + Y/PAAS patterns of the CD-1 marine carbonates are: (i) the composition of primitive South Atlantic seawater itself; or (ii) diagenesis. The paleogeography of the primitive South Atlantic Ocean in Aptian –Albian times (Fig. 01A), as a narrow Tethyan gulf (Dias-Brito, 2000), represented much higher continental/seawater proportion compared to open oceanic conditions. Additionally, enhanced global greenhouse conditions and continental weathering were attributed to Aptian-Albian transition, in times of the oceanic anoxic event (OAE 1b). These major oceanic-climate changes were observed in CD-1 section, through the increasing $^{87}Sr/^{86}Sr$ ratios (0.7072 to 0.7074), organic-matter preservation, and terrigenous content to the top of section (Caetano-Filho et al., 2017). The restricted South Atlantic seawater could have retained REE + Y patterns from continental sources, and consequently presented reduced REE + Y fractionation. However, Lawrence and Kamber (2006) showed that typical seawater REE + Y signatures, such as positive La anomaly, superchondritic Y/Ho ratios, and relative HREE enrichment over LREE, are already developed in the estuarine mixing zone. Preferential REE + Y release from the suspended river particles following the sequence La > Y > Ce > Pr > LREE > MREE > HREE, and, inversely, the preferential removal following LREE > MREE > HREE > Y > La by iron oxy-hydroxides

Table 3
Shale-normalized REE parameters calculated for the carbonates of CD-1 section.

Depth (mbsf)	MA	La/La*	Ce/Ce*	Eu/Eu*	Y/Ho	$(Dy/Sm)_n$	$(Nd/Yb)_n$	$(Pr/Yb)_n$	$(Pr/Tb)_n$	$(Tb/Yb)_n$
5346.8	MA-5	0.76	0.89	1.26	36.66	0.93	1.44	1.35	0.83	1.63
5365.1	MA-5	0.71	0.77	1.25	36.70	1.08	1.19	1.36	1.05	1.30
5365.8	MA-5	0.76	0.87	1.20	34.55	1.08	1.12	1.23	0.98	1.25
5377.5	MA-4	1.18	1.02	1.22	48.11	1.38	1.10	1.15	0.92	1.25
5399.6	MA-5	1.03	1.15	1.15	42.12	1.01	1.12	1.12	0.89	1.26
5413.5	MA-5	0.78	0.83	1.14	37.94	0.89	1.30	1.31	0.93	1.42
5423.2	MA-4	1.19	1.74	1.09	43.02	0.90	1.16	1.21	1.00	1.21
5456.0	MA-4	0.91	0.97	1.24	39.06	0.91	1.35	1.37	1.03	1.33
5460.4	MA-4	0.96	1.00	1.27	42.40	1.10	1.24	1.28	1.03	1.24
5499.1	MA-3	0.96	0.85	1.15	38.08	0.93	1.29	1.30	1.01	1.28
5512.0	MA-4	1.25	0.93	1.21	40.64	0.99	1.09	1.13	1.03	1.10
5544.2	MA-4	1.07	1.05	1.23	38.96	0.76	1.81	1.89	1.29	1.47
5558.3	MA-3	1.04	0.85	1.14	34.17	0.78	1.53	1.57	1.14	1.38
5620.0	MA-1	1.05	0.82	1.03	30.99	0.69	2.04	2.15	1.32	1.63
5629.3	MA-1	1.22	0.80	1.27	35.00	0.62	2.57	2.79	1.61	1.73
5634.9	MA-2	1.33	1.13	1.15	32.79	0.72	2.18	2.25	1.21	1.85
5638.5	MA-2	1.31	1.22	1.11	35.90	0.66	1.98	2.08	1.52	1.37
5644.8	MA-1	1.22	1.13	1.13	32.43	0.75	1.76	1.83	1.20	1.52

at mid-salinity zone are responsible for these signatures. They also observed a direct correlation between La concentration and Y/Ho ratios with salinity. Previous studies also showed this marine REE + Y fractionation in other coastal environments (e.g. Elderfield and Sholkovitz, 1987). Furthermore, considering the REE-carbonate complexation as the main factor controlling REE + Y fractionation in aqueous solutions (Cantrell and Byrne, 1987; Johannesson and Lyons, 1994) and the paleoenvironmental reconstructions for the late Aptian-early Albian early South Atlantic, a predominantly carbonate environment still in hypersaline conditions after the extensive Aptian evaporite deposition (Dias-Brito and Azevedo, 1986; Dias-Brito, 1987; Natland, 1978), it is unlikely that the expected seawater REE + Y fractionation would have not developed in the upper water column, at least at more distal domains of the carbonate platform (MA-3, MA-4, and MA-5).

Finally, in recent restricted stagnant basins, as Cariaco Basin (De Baar et al., 1988) and Black Sea (German et al., 1991), superficial waters present same shale-normalized REE + Y patterns of open oceanic conditions. These observations also suggest that the non-marine REE + Y signatures of our carbonate samples probably do not reflect the water column chemistry of the early South Atlantic. Furthermore, the main implication of these studies for our interpretations is related to the attenuation of seawater REE + Y pattern through suboxic (Black

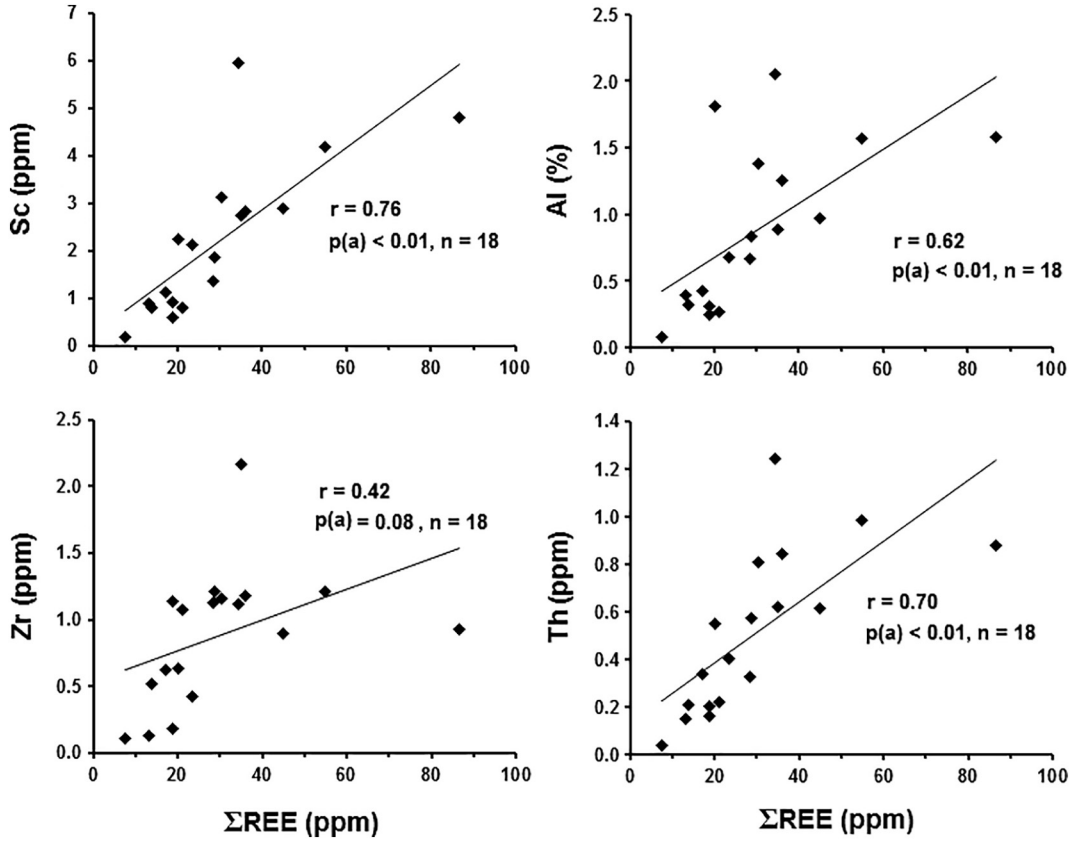

Fig. 3. Geochemical diagrams for the evaluation of the carbonate REE contents from the CD-1 section. Sc, Al, Zr, and Th are used as trackers for shale contamination over the primary REE seawater signature (e.g. Nothdurft et al., 2004; Frimmel, 2009).

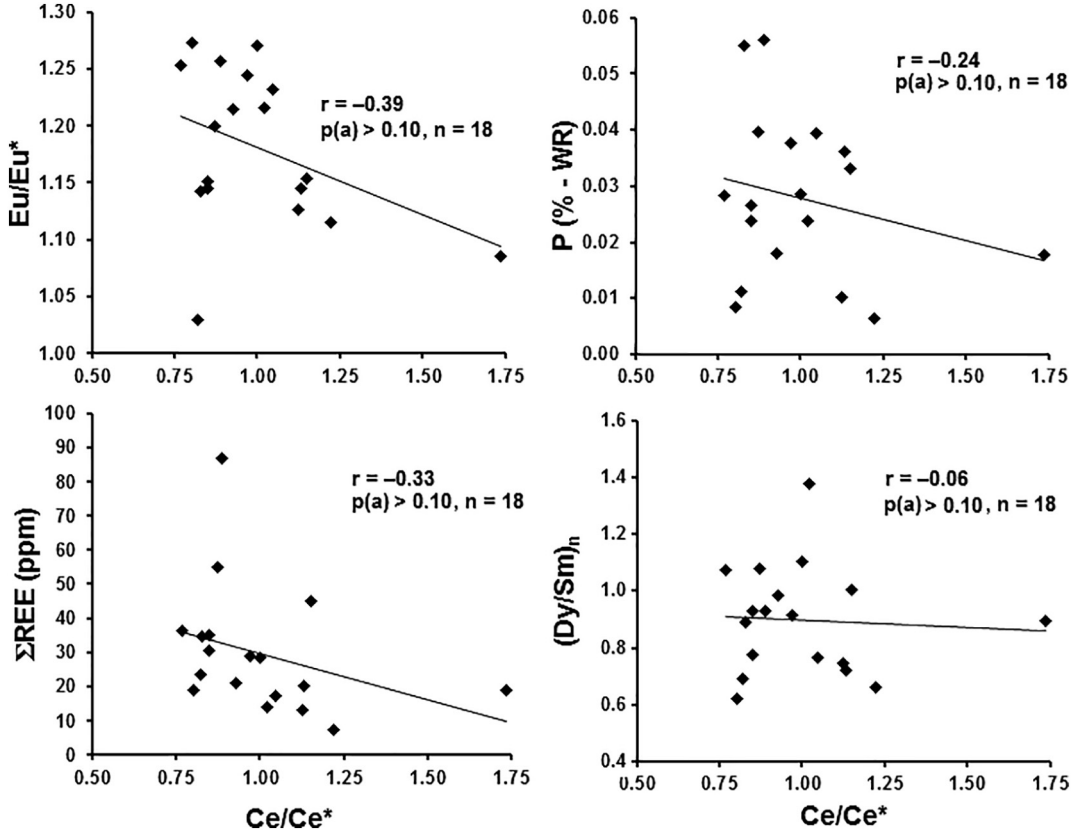

Fig. 4. Geochemical diagrams for evaluation of post-depositional alterations of Ce anomaly in carbonates, based on Shields and Stille (2001) and Pattan et al. (2005).

Sea, German et al., 1991) to anoxic (Cariaco Basin, De Baar et al., 1988) water column, represented by decreasing of HREE enrichment, as well as the inversion of negative Ce anomaly. Ce follows the Mn redox-controlled geochemical cycle in these conditions, as their reduction leads to dissolved phases in seawater. The LREE release, which are strictly trivalent and not redox sensitive, are controlled by secondary desorption process due to dissolution of Fe—Mn oxy-hydroxide coatings, as the main REE carriers (De Baar et al., 1988; German and Elderfield, 1989; German et al., 1991). These effects can be extended to sediments under anoxic early diagenesis, also linked to recycling of organic compounds, and represent an important role in REE marine cycling (Elderfield and Sholkovitz, 1987; De Baar et al., 1988; Haley et al., 2004; Kim et al., 2012; Piper and Bau, 2013). Elderfield and Sholkovitz (1987) showed an increase in the REE contents in reducing pore waters compared to the overlying seawater in a nearshore environment, suggesting that REE are remobilized during anoxic early diagenesis. Pore waters become enriched in LREE with increasing sediment depth and the more acid-labile fraction of the sediment (e.g. carbonates) also presented shale-normalized REE + Y patterns enriched in LREE with no fractionation compared to the bulk sediment, suggesting early diagenesis overprinting (German and Elderfield, 1990). Other studies also showed REE enrichment in pore waters and REE remobilization during anoxic early diagenesis, i.e., attenuation of HREE-enriched seawater pattern (e.g. German and Elderfield, 1989; Haley et al., 2004; Kim et al., 2012). These patterns are very similar to the CD-1 carbonates.

Anoxic bottom water conditions were considered a prevailing feature in South Atlantic during late Aptian-early Albian, due to restricted circulation patterns (Bolli et al., 1978; Hart and Koutsoukos, 2015; Herbin et al., 1987; Koutsoukos et al., 1991; Magniez-Jannin and Muller, 1987; Liu et al., 1988), and the influence of global ocean-climate changes associated with ocean anoxic events (e.g. Caetano-Filho et al., 2017; Koutsoukos et al., 1991; Tedeschi et al., 2017). Based on these paleoceanographic reconstructions and the overall anoxic early diagenesis attributed to the CD-1 carbonate microfacies associations (Caetano-Filho et al., 2017), the non-marine LREE-enriched patterns obtained are interpreted to be result of REE recycling and remobilization under reducing pore waters, or even in anoxic bottom water conditions.

5.2. *Paleoenvironmental implications of the carbonate REE + Y signatures from the primitive South Atlantic Ocean*

5.2.1. *Ce anomalies*

Several studies have demonstrated the clearly redox control over Ce geochemistry in seawater and marine depositional environments (De Baar et al., 1988; Elderfield and Greaves, 1982; Elderfield and Sholkovitz, 1987; German and Elderfield, 1989; German et al., 1991; Piper, 1974b; Piper and Bau, 2013; Schijf et al., 1991; Zhang and Nozaki, 1996, 1998). In authigenic minerals formed under oxygenated waters, this redox relationship would be direct, with Fe—Mn oxy-hydroxides phases presenting positive Ce anomalies, by Ce oxidation and scavenge, and authigenic carbonates and phosphates with negative Ce anomalies from seawater (e.g. Pattan et al., 2005; Piper, 1974b; Piper and Bau, 2013). However, given the REE remobilization noticed under suboxic to anoxic conditions in stagnant bottom waters and/or early diagenesis, Ce anomalies from authigenic minerals (e.g. carbonates) may not be interpret as paleoredox proxy from the overlying seawater. Instead, they would reflect the local bottom environment conditions (Elderfield and Sholkovitz, 1987; German and Elderfield, 1990).

Restricted circulation patterns and stagnant anoxic bottom conditions are well distinguished for the primitive South Atlantic Ocean in Aptian-Albian times. In this interval, organic-rich deposits lacking benthic biota were identified in areas of Sergipe (Koutsoukos et al., 1991), Santos and Campos basins (Azevedo, 2004; Caetano-Filho et al., 2017; Dias-Brito, 1995; Tedeschi et al., 2017), Angola basin (Bolli et al.,

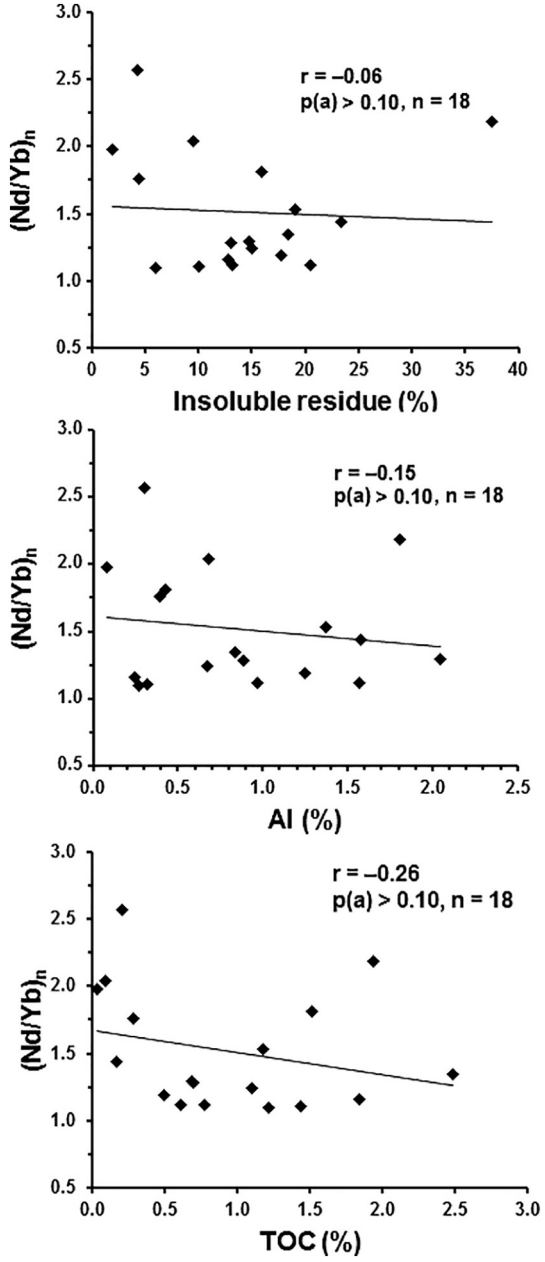

Fig. 5. Crossplots of insoluble residue vs. $(Nd/Yb)_n$, Al content vs. $(Nd/Yb)_n$, and TOC vs. $(Nd/Yb)_n$. LREE/HREE ratios are represented by the $(Nd/Yb)_n$ for monitoring relative LREE enrichments linked to contamination by detrital components, represented by insoluble residue, Al and TOC contents.

1978; Herbin et al., 1987; Magniez-Jannin and Muller, 1987; Ryan and Cita, 1977), and Falkland Plateau (Magniez-Jannin and Muller, 1987). This condition would have been a result of the initial South Atlantic Gulf paleogeography: the new sea was superficially connected with the North Atlantic, but essentially closed (or under minor influence) to the Meridional South Atlantic due the presence of an emergent barrier in its southern boundary, the São Paulo-Walvis Ridge (Arai, 2014; Azevedo, 2004; Dias-Brito, 2000; Koutsoukos et al., 1991; Natland, 1978).

Based on the Ce anomaly, some authors interpreted that reducing bottom conditions would persist in South Atlantic until ~ 56 Ma ago, by inversion of absent or positive Ce anomalies to negative Ce anomalies in carbonate sediments (Liu and Schmitt, 1984; Liu et al., 1988; Hu et al., 1988; Wang et al., 1986). These authors suggested that oxidizing conditions similar to the modern oceanic seawater were only developed after Late Paleocene, as a result of the final opening of South Atlantic Ocean and the establishment of deep water circulation due to subsidence of the main circulation barriers, São Paulo-Walvis Ridge at the south, and Romanche Fracture Zone at the north. German and Elderfield (1990) suggested another interpretation for the Ce anomaly turnover in the South Atlantic sedimentary record. They proposed that the absence or positive Ce anomalies in older carbonate sediments (> 54 Ma) were consequence of deposition in shallower continental shelf environments, in which diagenesis are usually suboxic to anoxic. This would result in sediments with REE signatures from reducing pore waters instead from the overlying seawater. Inversely, from the Late Paleocene to the present, the negative Ce anomaly in carbonates would represent oxic diagenesis in a deeper oceanic sedimentary environment. Nonetheless, German and Elderfield (1990) also associated the transition of shallower suboxic/anoxic to deeper oxic diagenectic environment and the subsequent Ce anomaly turnover in the South Atlantic to its final opening and open circulation conditions (~68 to 54 Ma). Therefore, the interpretations present for the Ce anomaly record in the South Atlantic are only slight different from each other and leads to a similar paleoceanographic inference.

In the present study, the virtually inexistent Ce anomaly for the CD-1 carbonates (Ce/Ce* average of 1.00 ± 0.22, median of 0.95 for the entire section) are in accordance with the previous Ce data for the early South Atlantic Ocean. The calculated anomalies are far higher from those of the modern oceanic waters (Table 3). They represent the earlier marine phase of this ocean during late Aptian-early Albian, with stagnant water mass condition and dominant anoxic early diagenesis, which could suppress the Ce anomaly from the overlying seawater by REE remobilization from other phases (e.g. German and Elderfield, 1989; Haley et al., 2004; Kim et al., 2012).

5.2.2. Y/Ho ratios

Although Y/Ho ratios for the analyzed carbonates are lower than the expected for modern seawater values, the evolution of this parameter through CD-1 section matches the transgression registered on the carbonate succession, with an increase in Y/Ho to the top of the section (Fig. 2). The more distal microfacies associations in the carbonate ramp, the higher average Y/Ho ratios (Table 3; Figs. 2 and 7), which may reflect the more effective scavenge of Ho compared to Y in seawater (Nozaki et al., 1997). The lower MA-5 Y/Ho ratios compared to MA-4 in the more distal part of paleoenvironmental reconstruction (Figs. 2 and 7) can be explained by the allochthonous nature of MA-5, composed of reworked sediments from more proximal parts of the carbonate ramp (Fig. 7). Thus, Y/Ho ratios of the carbonates of the CD-1 section are in agreement with the use of this proxy to point proximal vs. distal conditions (e.g. Frimmel, 2009; Nothdurft et al., 2004), although the relative abundances of these elements may have been smoothed by early diagenesis REE remobilization.

5.2.3. REE + Y/PAAS patterns

Most part of the CD-1 carbonate REE + Y/PAAS patterns are believed to represent early diagenetic signals of each depositional environment due to anoxic bottom conditions reconstructed for the primitive South Atlantic, based on microfacies analysis and organic-rich deposits (Bolli et al., 1978; Caetano-Filho et al., 2017; Hart and Koutsoukos, 2015; Herbin et al., 1987; Koutsoukos et al., 1991; Magniez-Jannin and Muller, 1987; Ryan and Cita, 1977; Tedeschi et al., 2017). REE + Y/PAAS patterns showed variations consistent with microfacies associations identified, disposed on the carbonate ramp model proposed for the CD-1 section (Fig. 6 and 7; Caetano-Filho et al., 2017).

MA-1 and MA-2 presented more pronounced shale-normalized LREE enrichment over HREE. Considering the more proximal environments for these microfacies (Fig. 7), composed of benthic-dominated wackestones and packstones (ostracodes and miliolids; Fig. 6A, B, and C), the first interpretation could be the major influence from continental waters (e.g. Frimmel, 2009; Nothdurft et al., 2004). However, they represent the lower part of CD-1 section (unit I) immediately above

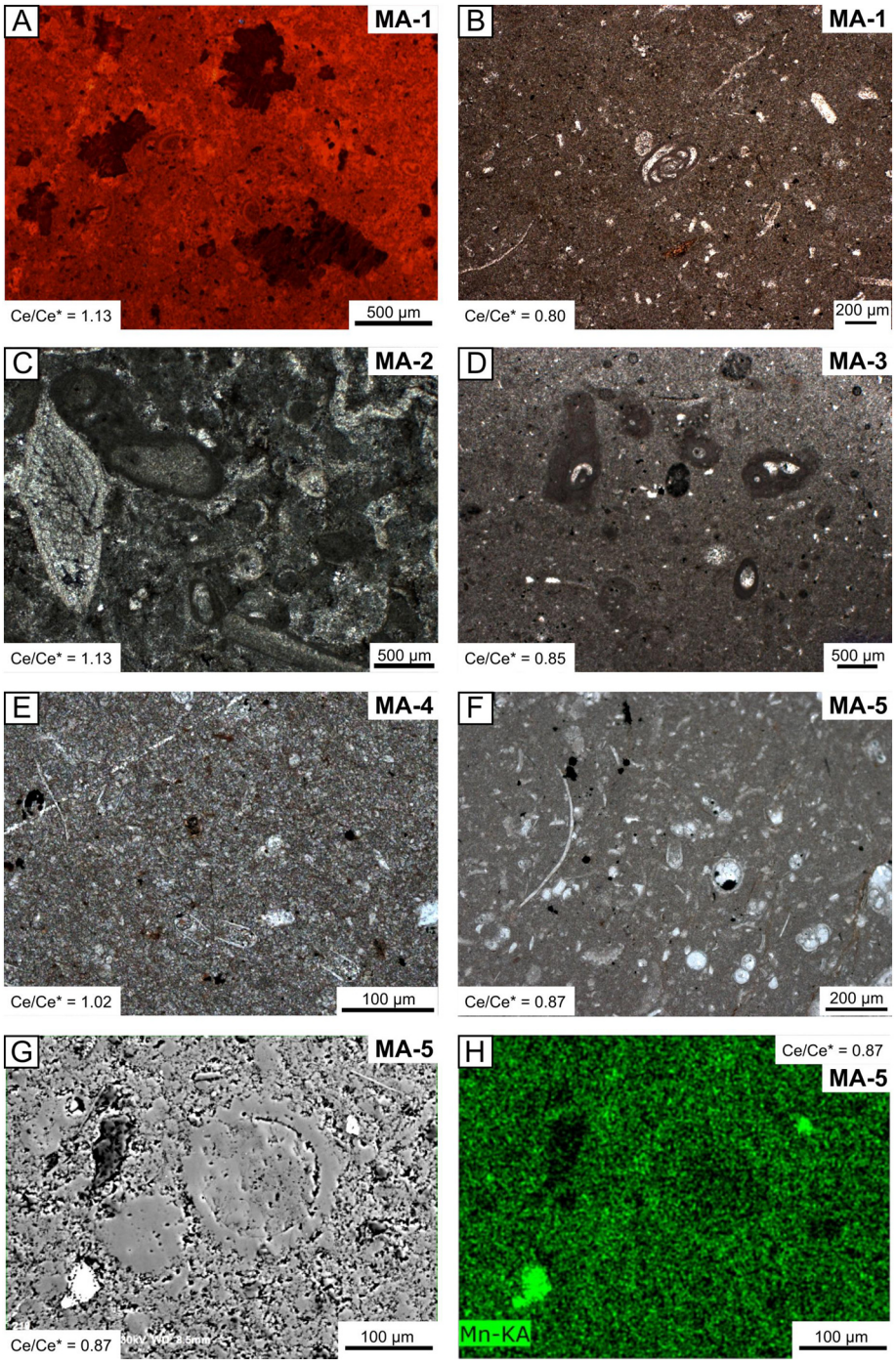

Fig. 6. Microfacies associations of the CD-1 section and Ce anomalies. A) Cathodoluminescence image of a crystalline and dolomitized limestone from MA-1 at the base of section (depth 5644.8 m); B) Bioclastic wackestone associated with MA-1, with benthic biota (milliolid at the centre); C) Bioclastic/peloidal packstone associated with MA-2; D) Bioclastic wackestone of MA-3 with bioturbation structures; E) Planktonic-dominated bioclastic wackestone with organic matter in the matrix; F, G and H) Bioclastic wackestone of MA-5 with abundance of reworked bioclasts and the presence of Fe—Mn oxy-hydroxides (white grain in G and brightest green in EDS image in H) and framboidal pyrite in the matrix (F). (For interpretation of the references to colour in this figure legend, the reader is referred to the web version of this article.)

evaporite deposits, still in a hypersaline environment under dry climate conditions. We interpreted this based on the lower detrital abundance (especially for the MA-1) and, consequently, lower REE contents (Table 1), and on the low diversity of biotic components (opportunistic organisms; Caetano-Filho et al., 2017), making difficult the interpretation of higher continental influence compared to the other CD-1 microfacies associations. On the other hand, the predominance of benthic biota and low organic matter in MA-1 and MA-2 argue against the interpretation of higher influence of suboxic to anoxic sulfidic early diagenesis over REE + Y/PAAS patterns. This behavior should be expected in the other microfacies associations which presented more evidences of anoxic sulfidic bottom conditions (absence of benthic biota, organic matter preservation, abundant framboidal pyrite; Figs. 2 and 6). Given the higher calcium carbonate content and higher compaction (base of section 5620 to 5650 mbsf – unit I; Fig. 2), carbonate rocks from MA-1 and MA-2 presented intense neomorphism processes (i.e. saddle dolomites, intense recrystallization; Fig. 6A) associated to a pronounced late burial diagenesis (Caetano-Filho et al., 2017). Thus, we interpret that these late diagenetic processes might have intensified the carbonate REE assimilation from the other phases (terrigenous siliciclastic, Fe—Mn oxy-hydroxides coatings, organic compounds) which preferentially scavenge LREE from seawater (e.g. Lawrence et al., 2006), leading to LREE-enriched shale-normalized patterns. Petrographic and geochemical evidences of burial diagenesis were reported for unit I, whereas MA-3, MA-4, and MA-5 present more preserved depositional textures, reflecting minor late burial diagenesis influence (Caetano-Filho et al., 2017).

MA-3 and MA-4 also presented a slight depletion in HREE, but with

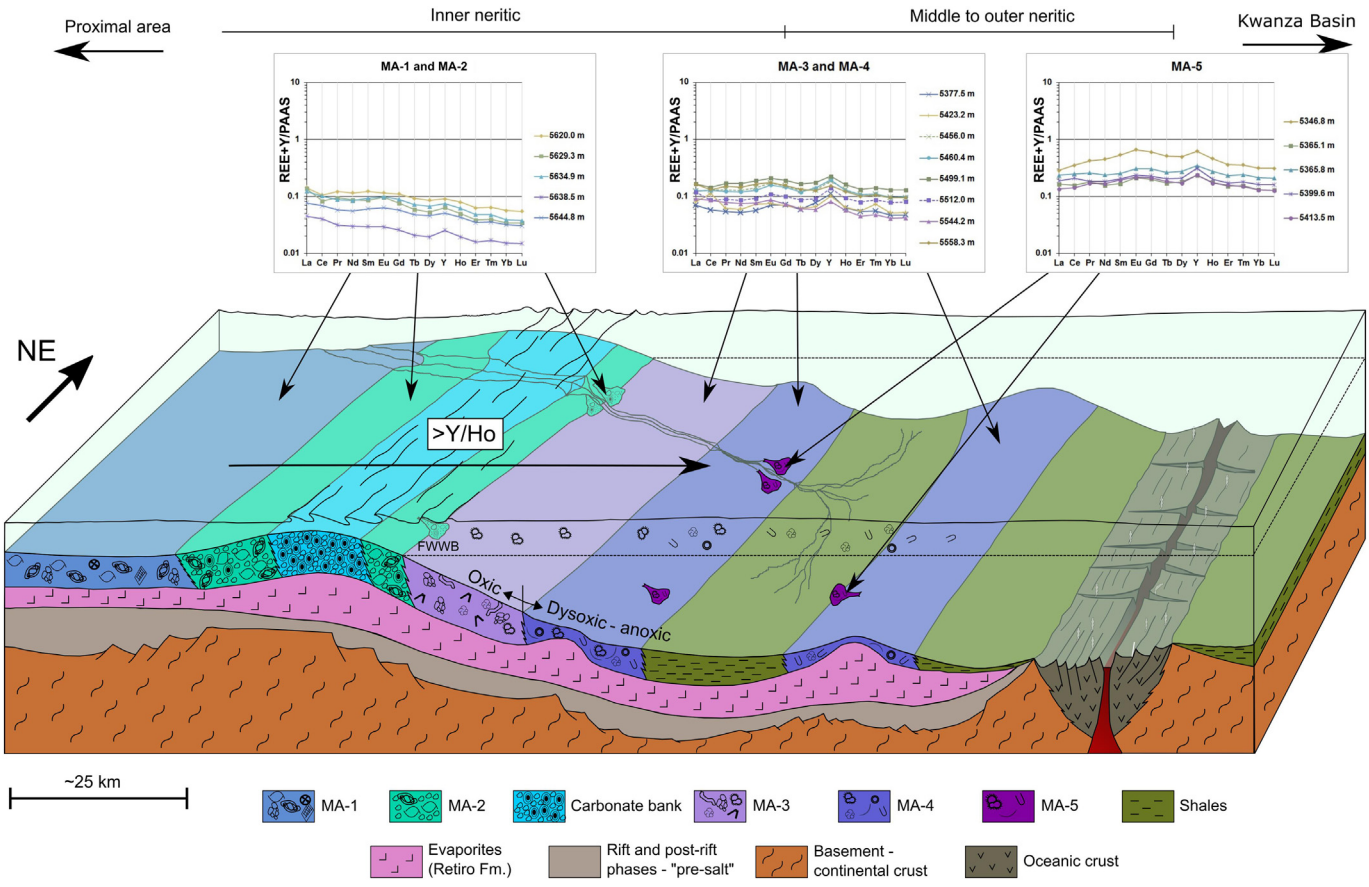

Fig. 7. Paleoenvironmental model for the CD-1 carbonate deposition in Campos Basin, based on microfacies analysis (Caetano-Filho et al., 2017). REE + Y/PAAS patterns found match microfacies association division and are related to respective diagenetic environments. Y/Ho ratios increase towards more distal portions of the platform.

flatter patterns compared with MA-1 and MA-2. These microfacies associations correspond to more distal facies, deposited in middle to outer neritic environment (Fig. 7). MA-3 present benthic biota and bioturbation structures pointing to primary oxygenated bottom conditions (Figs. 2, 6D, and 7). However, the early dysoxic to anoxic diagenesis might have been developed with increasing burial, as some framboidal pyrite, virtually inexistent Ce anomaly and relatively high TOC contents are observed in this microfacies associations (Table 1, Fig 6D). MA-4 is the most distal and frequent microfacies association observed through unit III (Fig. 2) and present some evidences of anoxic bottom conditions, such as the absence of benthic biota (only planktonic organisms; Fig. 6E), the highest TOC and HI values (Table 1; Fig. 2; Caetano-Filho et al., 2017), the most positive Ce anomaly (Table 3; Fig. 2), and the abundance of framboidal pyrite in the matrix (Fig. 6E), pointing to sulfidic early diagenetic conditions. The shale-normalized REE + Y patterns of the MA-3 and MA-4 are in accordance with previous studies observations in modern anoxic basins and reducing early diagenetic environments. They are a result of the REE benthic fluxes and remobilization from other mineralogical REE carrier phases (Fe—Mn oxy-hydroxides coatings in detrital sediments, organic compounds, etc.; Elderfield and Sholkovitz, 1987; German and Elderfield, 1989; Haley et al., 2004; Kim et al., 2012). Elderfield and Sholkovitz (1987) observed increased REE contents in pore water of reducing early diagenetic environment compared to the overlying seawater, and interpreted the LREE enrichment in pore waters as a diagenetic REE remobilization which would reflect in the LREE enriched patterns of sediments (German and Elderfield, 1990). Similarly, German and Elderfield (1989) presented continuous enrichment in LREE through the anoxic column in a seasonally anoxic basin, by desorption of REE(III) from particulate, which became more depleted in LREE. They also showed pore waters enriched in REE contents up to ten times compared to bottom waters. Following the study of Haley et al. (2004) in pore waters of marine sediments, Kim et al. (2012) showed flat REE + Y patterns for sulfidic zone within the sediment. These authors suggested that the major fraction of complexed REE is released at this zone. Therefore, the REE + Y/PAAS flat patterns of the MA-3 and MA-4 carbonates are compatible with the early anoxic and sulfidic diagenetic environment identified previously (below to oxic/dysoxic-anoxic interface within the sediment; Figs. 6 and 7; Caetano-Filho et al., 2017) and possible with stagnant oxygen-depleted waters of the primitive South Atlantic (Bolli et al., 1978; Koutsoukos et al., 1991; Natland, 1978; Ryan and Cita, 1977).

REE + Y/PAAS patterns of MA-5 correspond to a distinctive “MREE bulge” pattern (Haley et al., 2004) due to remarkable enrichment in MREE (Figs. 2 and 7). MA-5 is composed of tempestites (Fig. 6F, G and H), with unusual co-occurrence of glauconite grains, Fe—Mn oxy-hydroxides (Fig. 6G and H), and framboidal pyrite, as authigenic minerals, which reflect reworking from shallower and oxygenated bottom environments and transport to deeper and dysoxic to anoxic sulfidic environments (Caetano-Filho et al., 2017). Considering the final anoxic early diagenetic environment for MA-5 deposition (Figs. 6 and 7), Haley et al. (2004) reported similar REE + Y/PAAS patterns (“MREE bulge” pattern) for pore waters in which dissolution of Fe oxy-hydroxides under anoxic early diagenesis occurs. Pattan et al. (2005) also presented MREE-enriched REE + Y/PAAS patterns for bulk sediments containing Fe—Mn oxy-hydroxides, due to higher scavenge of MREE by these authigenic minerals in seawater. Therefore, we interpret the MREE-enriched REE + Y/PAAS patterns of MA-5 as influenced by REE remobilization from Fe—Mn oxy-hydroxides grains (Fig. 6G and H) to carbonate phases in a dysoxic to anoxic early diagenetic environment,

as long as Fe—Mn oxy-hydroxides grains were only observed in this microfacies association.

5.3. On the significance of shale-normalized REE + Y distribution in ancient carbonates and paleoenvironmental reconstructions

The REE + Y/PAAS patterns of marine carbonates from CD-1 section do not seem to reflect seawater patterns, as long as no "seawater type" patterns were developed throughout the distal facies of the carbonate ramp model (middle to outer neritic environment; Fig. 7), well-constrained by microfacies analysis (Caetano-Filho et al., 2017). Instead, the different REE + Y/PAAS patterns reflect the diagenetic environment influenced either by burial diagenesis (basal unit I – MA-1 and MA-2), early anoxic diagenesis (MA-3 and MA-4), or dissolution of Fe—Mn oxy-hydroxides grains in such conditions (MA-5). The early diagenetic overprint and LREE recycling also could explain the absence of dominant positive La anomalies and negative Ce anomalies in CD-1 marine carbonates, a common feature in seawater.

Stagnant anoxic basins, as the primitive South Atlantic or modern environments studied previously (Cariaco Trench, De Baar et al., 1988; Black Sea, German et al., 1991; Schijf et al., 1991), may be common marine analogous environments in the Precambrian record. Anoxic bottom/early diagenetic conditions were dominant before the final oxygenation of Earth's surface and the infauna diversification with appearance of vertical bioturbation, which is believed to have occurred at the end of Neoproterozoic Era (e.g. Canfield et al., 2007; Kah et al., 2004; Lyons et al., 2014; Seilacher et al., 2005). For the late Neoproterozoic basins, the paleogeography also favored restricted circulation patterns and the possible development of stagnant anoxic bottom conditions, related to final stage of tectonic cycles and continental settings (e.g. West Congolian Group, Southwestern Africa; Frimmel, 2009; Bambuí Group, Central-East Brazil; Martins and Lemos, 2007; Paula-Santos et al., 2017; Santos et al., 2000). Therefore, the shale-normalized REE + Y patterns of seawater could be suppressed in these cases (e.g. Elderfield and Sholkovitz, 1987; German and Elderfield, 1990; Holser, 1997), making the sole use of REE + Y as a paleoenvironmental proxy doubtful in the absence of other tools (e.g. microfacies analysis, biotic content). On the other hand, REE + Y signatures in ancient carbonate rocks show potential to track early diagenesis conditions and related metabolisms, also important to paleoceanographic reconstructions.

6. Conclusions

Carbonate REE + Y/PAAS compositions from the restricted early marine stage of South Atlantic Ocean did not present the expected "seawater" pattern, even considering the distal facies or more pure carbonate facies. Instead, they presented more flat shale-normalized distributions. Although the paleogeography of the primitive South Atlantic Ocean is represented as a Tethyan gulf, completely surrounded by continental masses, these REE + Y signatures were not interpreted as influenced by continental waters, based on observations that the typical seawater REE + Y fractionation occurs in modern epicontinental seas, estuarine, and coastal environments. On the other hand, distinct carbonate REE + Y/PAAS patterns matched the microfacies associations disposed on a carbonate ramp model and seem to reflect their respective dominant diagenetic environments, influenced by REE remobilization from detrital components as the main REE carriers in the marine setting (Fe—Mn oxy-hydroxides coatings and grains, organic matter, terrigenous siliciclastics). In summary: (i) MA-1 and MA-2 microfacies associations (inner ramp) presented pronounced LREE-enriched REE + Y/PAAS patterns, which reflect increased REE remobilization due to the intense burial diagenesis at the base of section; (ii) MA-3 and MA-4 (middle to outer ramp) presented flat REE + Y/PAAS patterns which were associated with the REE remobilization during the anoxic and sulfidic early diagenesis; and (iii) as resedimented deposits transported from shallower and oxygenated areas to deeper and anoxic sulfidic environments, MA-5 presented MREE-enriched shale-normalized REE + Y patterns, which were assigned to the dissolution of Fe—Mn oxy-hydroxides grains under anoxic early diagenesis. The virtually inexistent Ce anomalies of the studied carbonates are in agreement with previous studies that point to stagnant conditions for the South Atlantic Ocean carbonates until the Late Paleocene. Even attenuated compared with modern values, the Y/Ho ratios from CD-1 carbonates were in good agreement with paleoenvironmental conditions inferred through microfacies analysis, increasing towards the more distal microfacies. Caution is recommended with the sole use of REE + Y/PAAS patterns as paleoenvironmental proxy for ancient carbonate rocks, mainly in Precambrian successions lacking biotic components. The primitive South Atlantic Ocean, as a restricted and stagnant sea, corroborate some modern analogous observations of REE recycling under anoxic bottom/early diagenetic conditions, suppressing the shale-normalized REE + Y signatures of the overlying seawater. These conditions were probably quite common before the final Earth's surface oxygenation during the late Neoproterozoic Era and the advent of infauna bioturbation through Ediacaran-Cambrian transition.

Acknowledgments

This study was supported by the project "Carbonate rocks of Brazil", a partnership between São Paulo State University (UNESP) and PETROBRAS (grant #0050.0051732.09.9 Petrobras/Unesp/Fundunesp). The first author currently holds a São Paulo Research Foundation (FAPESP) scholarship (grant #2016/11496-5). Dr. Gustavo M. Paula-Santos holds a São Paulo Research Foundation (FAPESP) scholarship (grant #2017/00399-1). We are grateful to the staff of Center for Petroleum Geosciences – UNESPetro and Geochemistry Laboratory of Petrology and Metallogeny Department, UNESP; Chemical Stratigraphy and Organic Geochemistry Laboratory, Rio de Janeiro State University (UERJ); and Geoanalítica-USP Facility, University of São Paulo (USP), especially to Dra. Sandra Andrade; for supporting REE data acquisition. We also thank to Dra. Sylvia dos Anjos, Dr. Rogério Antunes, and MSc. Adali Spadini (Petrobras) for all the support and to Dr. Ricardo L. M. de Azevedo and Dr. René Rodrigues for the assistance during the whole project. Finally, we thank to the two anonymous reviewers for the suggestions that improved this manuscript.

References

Alibo, D.S., Nozaki, Y., 1999. Rare earth elements in seawater: particle association, shale-normalization, and Ce oxidation. Geochim. Cosmochim. Acta 63, 363–372. http://dx.doi.org/10.1016/S0016-7037(98)00279-8.

Arai, M., 2014. Aptian/Albian (Early Cretaceous) paleogeography of the South Atlantic: a paleontological perspective. Brazilian J. Geol. 44, 339–350. http://dx.doi.org/10.5327/Z2317-4889201400020012.

Azevedo, R., 2004. Paleoceanografia ea evolução do Atlantico Sul no Albiano. Bol. Geociências da Petrobras 231–249.

Bau, M., Dulski, P., 1996. Distribution of yttrium and rare-earth elements in the Penge and Kuruman iron-formations, Transvaal Supergroup, South Africa. Precambrian Res. 79, 37–55. http://dx.doi.org/10.1016/0301-9268(95)00087-9.

Bau, M., Dulski, P., Möller, P., 1995. Yttrium and holmium in South Pacific seawater: vertical distribution and possible fractionation mechanisms. Chem. Erde 55, 1–15.

Bertram, C.J., Elderfield, H., 1993. The geochemical balance of the rare earth elements and neodymium isotopes in the oceans. Geochim. Cosmochim. Acta 57, 1957–1986. http://dx.doi.org/10.1016/0016-7037(93)90087-D.

Blanco-Bustamante, S., 2001. Biocronologia del Cretacico medio de Cuba Central de acuerdo a microfosiles planctonicos: su relacion con el paleoambiente. In: IV Congresso de Geologia y Mineria, Estratigrafía, Paleontología y Sedimentología, La Habana. Memorias Geomin, pp. 31–39.

Bodin, S., Meissner, P., Janssen, N.M.M., Steuber, T., Mutterlose, J., 2015. Large igneous provinces and organic carbon burial: controls on global temperature and continental weathering during the Early Cretaceous. Glob. Planet. Chang. 133, 238–253. http://dx.doi.org/10.1016/j.gloplacha.2015.09.001.

Bolhar, R., Van Kranendonk, M.J., 2007. A non-marine depositional setting for the northern Fortescue Group, Pilbara Craton, inferred from trace element geochemistry of stromatolitic carbonates. Precambrian Res. 155, 229–250. http://dx.doi.org/10.1016/j.precamres.2007.02.002.

Bolli, H.M., Ryan, W.B.F., Foresman, J.B., Hottman, W.E., Kagami, H., Longoria, J.F., Mcknight, B.K., Melguem, M., Natland, J., Proto-Decima, F., Siesser, W.G., 1978. Angola continental margin e sites 364 and 365. In: Bolli, H.M., Ryan, W.B.F. (Eds.), Initial Reports of the Deep Sea Drilling Project, 40. United States Government Printing Office, Washington D.C., USA, pp. 357–455.

Bralower, T.J., Fullagar, P.D., Paull, C.K., Dwyer, G.S., Leckie, R.M., 1997. Mid-cretaceous strontium-isotope stratigraphy of deep-sea sections. Geol. Soc. Am. Bull. 109 (10), 1421–1442.

Caetano-Filho, S., Dias-Brito, D., Rodrigues, R., Azevedo, R.L.M., 2017. Carbonate microfacies and chemostratigraphy of a late Aptian-early Albian marine distal section from the primitive South Atlantic (SE Brazilian continental margin): record of global ocean-climate changes? Cretac. Res. 74, 23–44. http://dx.doi.org/10.1016/j.cretres.2017.02.011.

Canfield, D.E., Poulton, S.W., Narbonne, G.M., 2007. Late-neoproterozoic deep-ocean oxygenation and the rise of animal life. Science 315, 92–95. http://dx.doi.org/10.1126/science.1135013.

Cantrell, K.J., Byrne, R.H., 1987. Rare earth elements complexation by carbonate and oxalate ions. Geochim. Cosmochim. Acta 51, 597–605.

Carvalho, M.D., Dias-Brito, D., Ferré, B., 1999. Bacia de Jequitinhonha e novas indicações de águas tetianas no Atlântico Sul. In: Boletim do 5° Simpósio do Cretáceo do Brasil, Rio Claro, Brazil, pp. 643–649.

Chang, H.K., Kowsmann, R.O., 1987. Interpretação genética das sequências estratigráficas das bacias da margem continental Brasileira. Rev. Bras. Geosci. 17 (2), 74–80.

Chen, S., Gui, H., Sun, L., 2014. Geochemical characteristics of REE in the Late Neoproterozoic limestone from northern Anhui Province, China. Chin. J. Geochem. 33, 187–193. http://dx.doi.org/10.1007/s11631-014-0677-z.

De Baar, H.J.W., Bacon, M.P., Brewer, P.G., Bruland, K.W., 1985. Rare earth elements in the Pacific and Atlantic Oceans. Geochim. Cosmochim. Acta 49, 1943–1959. http://dx.doi.org/10.1016/0016-7037(85)90089-4.

De Baar, H.J.W., German, C.R., Elderfield, H., van Gaans, P., 1988. Rare earth element distributions in anoxic waters of the Cariaco Trench. Geochim. Cosmochim. Acta 52, 1203–1219. http://dx.doi.org/10.1016/0016-7037(88)90275-X.

Delpomdor, F., Blanpied, C., Virgone, A., Préat, A., 2013. Paleoenvironments in meso-neoproterozoic carbonates of the Mbuji-Mayi supergroup (Democratic Republic of Congo) - microfacies analysis combined with C-O-Sr isotopes, major-trace elements and REE + Y distributions. J. Afr. Earth Sci. 88, 72–100. http://dx.doi.org/10.1016/j.jafrearsci.2013.09.002.

Dias-Brito, D., 1987. A Bacia de Campos no Mesocretáceo: uma contribuição à paleoceanografia do Atlântico Sul Primitivo. Rev. Bras. Geosci. 17 (2), 162–167.

Dias-Brito, D., 1994. Comparação dos carbonatos pelágicos do Cretáceo médio da Margem Atlântica Brasileira com os do Golfo do México: novas evidências do Tétis Sul-Atlantiano. In: Boletim do 3° Simpósio sobre o Cretáceo do Brasil, Rio Claro, Brazil, pp. 11–18.

Dias-Brito, D., 1995. Calcisferas e microfácies em rochas carbonáticas pelágicas mesocretáceas (Doctorate thesis). Universidade Federal do Rio Grande do Sul. Porto Alegre, Brazil (688 pp).

Dias-Brito, D., 1999. Usando pitonelidos e colomielidos para dividir o Albiano: um estudo a partir da margem sudeste do Brasil. In: Boletim do 5° Simpósio sobre o Cretáceo do Brasil, Rio Claro, Brazil, pp. 627–635.

Dias-Brito, D., 2000. Global stratigraphy, palaeobiogeography and palaeoecology of Albian-Maastrichtian pithonellid calcispheres: impact on Tethys configuration. Cretac. Res. 21 (2–3), 315–349.

Dias-Brito, D., Azevedo, R.L.M., 1986. As sequências deposicionais marinhas da Bacia de Campos sob a ótica paleoecológica. In: Congresso Brasileiro de Geologia 34. Brazil. Anais 1, Goiânia, pp. 38–48.

Dias-Brito, D., Ferré, B., 2001. Roveacrinids (stemless crinoids) in the Albian carbonates of the offshore Santos Basin, southeastern Brazil: stratigraphic, palaeobiogeographic and palaeoceanographic significance. J. S. Am. Earth Sci. 14 (2), 203–218.

Elderfield, H., Greaves, M.J., 1982. The rare earth elements in seawater. Nature 296, 214–219. http://dx.doi.org/10.1038/296214a0.

Elderfield, H., Sholkovitz, E.R., 1987. Rare earth elements in the pore waters of reducing nearshore sediments. Earth Planet. Sci. Lett. 82, 280–288.

Erbacher, J., Hemleben, C., Huber, B.T., Markey, M., 1999. Correlating environmental changes during early Albian oceanic anoxic event 1B using benthic foraminiferal paleoecology. Mar. Micropaleontol. 38, 7–28. http://dx.doi.org/10.1016/S0377-8398(99)00036-5.

Erbacher, J., Huber, B.T., Norris, R.D., Markey, M., 2001. Increased thermohaline stratification as a possible cause for an ocean anoxic event in the Cretaceous period. Nature 409, 325–327. http://dx.doi.org/10.1038/35053041.

Esteves, F.R., Spadini, A.R., Saito, M., 1987. A sedimentação Albo-Turoniana (Formação Macaé) da Bacia de Campos. In: Simpósio de Geologia Regional 1, Rio de Janeiro, Brazil. Anais, pp. 27–42.

Frimmel, H.E., 2009. Trace element distribution in Neoproterozoic carbonates as palaeoenvironmental indicator. Chem. Geol. 258, 338–353. http://dx.doi.org/10.1016/j.chemgeo.2008.10.033.

German, C.R., Elderfield, H., 1989. Rare earth elements in Saanich Inlet, British Columbia, a seasonally anoxic basin. Geochim. Cosmochim. Acta 53, 2561–2571.

German, R., Elderfield, H., 1990. Laboratory, Wormley, Godaiming, United Kingdom. 5, 823–833.

German, C.R., Holliday, B.P., Elderfield, H., 1991. Redox cycling of rare earth elements in the suboxic zone of the Black Sea. Geochim. Cosmochim. Acta 55, 3553–3558.

German, C.R., Masuzawa, T., Greaves, M.J., Elderfield, H., Edmond, J.M., 1995. Dissolved rare earth elements in the Southern Ocean: cerium oxidation and the influence of hydrography. Geochim. Cosmochim. Acta 59, 1551–1558. http://dx.doi.org/10.1016/0016-7037(95)00061-4.

González-León, C.M., Scott, R.W., Löser, H., Lawton, T.F., Robert, E., Valencia, V.A., 2008. Upper Aptian-Lower Albian Mural Formation: stratigraphy, biostratigraphy and depositional cycles on the Sonoran shelf, northern México. Cretac. Res. 29, 249–266. http://dx.doi.org/10.1016/j.cretres.2007.06.001.

Guardado, L.R., Gamboa, L.A.P., Luchesi, C.F., 1989. Petroleum geology of the Campos Basin, a model for a producing Atlantic type basin. In: Edwards, J.D., Santogrossi, P.A. (Eds.), Divergent/Passive Margin Basins, AAPG Memoir, Tulsa 48, pp. 3–79.

Haley, B.A., Klinkhammer, G.P., McManus, J., 2004. Rare earth elements in pore waters of marine sediments. Geochim. Cosmochim. Acta 68, 1265–1279. http://dx.doi.org/10.1016/j.gca.2003.09.012.

Hart, M.B., Koutsoukos, E.A.M., 2015. Paleoecology of cretaceous foraminifera: examples from the Atlantic Ocean and Gulf of Mexico. Region 175–199.

Herbin, J.P., Muller, C., Graciansky, P.C., Jacquin, T., Magniez-Jannin, F., Unternehr, P., 1987. Cretaceous anoxic events in the South Atlantic. Rev. Bras. Geosci. 17 (2), 92–99.

Herrle, J.O., Kößler, P., Friedrich, O., Erlenkeuser, H., Hemleben, C., 2004. High-resolution carbon isotope records of the Aptian to Lower Albian from SE France and the Mazagan Plateau (DSDP Site 545): a stratigraphic tool for paleoceanographic and paleobiologic reconstruction. Earth Planet. Sci. Lett. 218, 149–161. http://dx.doi.org/10.1016/S0012-821X(03)00646-0.

Herrle, J.O., Schröder-Adams, C.J., Davis, W., Pugh, A.T., Galloway, J.M., Fath, J., 2015. Mid-cretaceous high arctic stratigraphy, climate, and oceanic anoxic events. Geology 43, 403–406. http://dx.doi.org/10.1130/G36439.1.

Holser, W.T., 1997. Evaluation of the application of rare-earth elements to paleoceanography. Palaeogeogr. Palaeoclimatol. Palaeoecol. 132, 309–323. http://dx.doi.org/10.1016/S0031-0182(97)00069-2.

Hu, X., Wang, Y.L., Schmitt, R.A., 1988. Geochemistry of sediments on the Rio Grande Rise and the redox evolution of the South Atlantic Ocean. Geochim. Cosmochim. Acta 52, 201–207. http://dx.doi.org/10.1016/0016-7037(88)90068-3.

Jiedong, Y., Weiguo, S., Zongzhe, W., Yaosong, X., Xiancong, T., 1999. Variations in Sr and C isotopes and Ce anomalies in successions from China: evidence for the oxygenation of Neoproterozoic seawater? Precambrian Res. 93, 215–233. http://dx.doi.org/10.1016/S0301-9268(98)00092-8.

Johannesson, K.H., Lyons, W.B., 1994. The rare earth element geochemistry of Mono Lake water and the importance of carbonate complexing. Limnol. Oceanogr. 39, 1141–1154. http://dx.doi.org/10.4319/lo.1994.39.5.1141.

Jones, C.E., Jenkyns, H.C., 2001. Seawater strontium isotopes, oceanic anoxic events, and seafloor hydrothermal activity in the Jurassic and Cretaceous. Am. J. Sci. 301, 112–149.

Kah, L.C., Lyons, T.W., Frank, T.D., 2004. Low marine sulphate and protracted oxygenation of the Proterozoic biosphere. Nature 431, 834–838. http://dx.doi.org/10.1038/nature02974.

Kamber, B.S., Greig, A., Collerson, K.D., 2005. A new estimate for the composition of weathered young upper continental crust from alluvial sediments, Queensland, Australia. Geochim. Cosmochim. Acta 69, 1041–1058. http://dx.doi.org/10.1016/j.gca.2004.08.020.

Kennedy, W.J., Gale, A.S., Huber, B.T., Petrizzo, M.R., Bown, P., Barchetta, A., Jenkyns, H.C., 2014. Integrated stratigraphy across the Aptian/Albian boundary at Col de Pré-Guittard (southeast France): a candidate global boundary stratotype section. Cretac. Res. 51, 248–259. http://dx.doi.org/10.1016/j.cretres.2014.06.005.

Kim, J.H., Torres, M.E., Haley, B.A., Kastner, M., Pohlman, J.W., Riedel, M., Lee, Y.J., 2012. The effect of diagenesis and fluid migration on rare earth element distribution in pore fluids of the northern Cascadia accretionary margin. Chem. Geol. 291, 152–165. http://dx.doi.org/10.1016/j.chemgeo.2011.10.010.

Koutsoukos, E.A.M., Mello, M.R., Azambuja Filho, N.C., Hart, M.B., Maxwell, J.R., 1991. The Upper AptianeAlbian succession of the Sergipe Basin, Brazil: an integrated paleoenvironmental assessment. AAPG Bull. 75, 479–498.

Lawrence, M.G., Kamber, B.S., 2006. The behaviour of the rare earth elements during estuarine mixing-revisited. Mar. Chem. 100, 147–161. http://dx.doi.org/10.1016/j.marchem.2005.11.007.

Lawrence, M.G., Greig, A., Collerson, K.D., Kamber, B.S., 2006. Rare earth element and yttrium variability in South East Queensland waterways. Aquat. Geochem. 12, 39–72. http://dx.doi.org/10.1007/s10498-005-4471-8.

Ling, H.-F., Chen, X., Li, D., Wang, D., Shields-Zhou, G.A., Zhu, M., 2013. Cerium anomaly variations in Ediacaran–earliest Cambrian carbonates from the Yangtze Gorges area, South China: implications for oxygenation of coeval shallow seawater. Precambrian Res. 225, 110–127. http://dx.doi.org/10.1016/j.precamres.2011.10.011.

Liu, Y.G., Schmitt, R.A., 1984. Chemical profiles in sediment and basalt samples from Deep Sea Drilling Project LEG 74, hole 525A, Walvis Ridge. In: Moore Jr.T.C., Rabinowitz, P.D. (Eds.), Initial Reports of the Dep Sea Drilling Project, 74. US Government Printing Office, Washington, DC, pp. 713–730. http://dx.doi.org/10.2973/dsdp.proc.74.123.1984.

Liu, Y.G., Miah, M.R.U., Schmitt, R.A., 1988. Cerium: a chemical tracer for paleo-oceanic redox conditions. Geochim. Cosmochim. Acta 52, 1361–1371. http://dx.doi.org/10.1016/0016-7037(88)90207-4.

Longoria, J.F., Monreal, R., 2009. The use of planktonic microfossils to resolve chronostratigraphic, tectonic, and paleogeographic uncertainties in the Lower Cretaceous of eastern Sonora, NW Mexico. In: Geologic Problem Solving with Microfossils: A Volume in Honor of Garry D. Jones. 93. SEPM Special Publication, pp. 269–285.

Lyons, T.W., Reinhard, C.T., Planavsky, N.J., 2014. The rise of oxygen in Earth's early ocean and atmosphere. Nature 506, 307–315. http://dx.doi.org/10.1038/nature13068.

Madhavaraju, J., Sial, A.N., González-León, C.M., Nagarajan, R., 2013. Carbon and oxygen isotopic variations in early albian limestone facies of the mural formation, pitaycachi section, northeastern Sonora. Mexico. Rev. Mex. Ciencias Geol. 30, 526–539.

Magniez-Jannin, F., Muller, C., 1987. Cretaceous stratigraphic and paleoenvironmental

data from the South Atlantic (foraminifers and nannoplankton). Rev. Bras. Geosci. 17 (2), 100–105.
Martins, M., Lemos, V.B., 2007. Análise estratigráfica das sequências neoproterozoicas da Bacia do São Francisco. Rev. Bras. Geosci. 37 (4), 156–167.
McLennan, S.M., 1989. Rare earth elements in sedimentary rocks: influence of provenance and sedimentary process. Rev. Mineral. Geochem. 21, 169–200.
Michalík, J., Lintnerová, O., Reháková, D., Boorová, D., Šimo, V., 2012. Early Cretaceous sedimentary evolution of a pelagic basin margin (the Manín Unit, central Western Carpathians, Slovakia). Cretac. Res. 38, 68–79. http://dx.doi.org/10.1016/j.cretres.2012.02.006.
Moffett, J.W., 1990. Microbially mediated cerium oxidation in seawater. Nature 345, 421–423.
Mohriak, W.U., 2004. Recursos energéticos associados à ativação tectônica mesozoico-cenozoica da America do sul. In: Mantesso-Neto, V., Bartorelli, A., Carneiro, C.D.R., Brito-Neves, B.B. (Eds.), Geologia do continente sulamericano: evolução da obra de Fernando Flávio Marques de Almeida. Beca, São Paulo, pp. 293–318.
Mohriak, W.U., 2009. Tectônica de sal autóctone e alóctone na margem sudeste brasileira. In: Mohriak, W.U., Szatmari, P., Anjos, S.M.C. (Eds.), Sal: Geologia e Tectônica. Beca, São Paulo, pp. 302–315.
Natland, J.H., 1978. Composition, Provenance, and Diagenesis of Cretaceous Clastic Sediments Drilled on the Atlantic Continental Rise off Southern Africa, DSDP Site 361 - Implications for the Early Circulation of the South Atlantic. Cover. Leg 40 Cruises Drill. Vessel Glomar Chall. Cape Town, South Africa to Abidjan, Ivory Coast. 40. pp. 1025–1061.
Nothdurft, L.D., Webb, G.E., Kamber, B.S., 2004. Rare earth element geochemistry of Late Devonian reefal carbonates, canning basin, Western Australia: confirmation of a seawater REE proxy in ancient limestones. Geochim. Cosmochim. Acta 68 (2), 263–283.
Nozaki, Y., 2001. Rare earth elements and their isotopes in the ocean. Encycl. Ocean Sci. 2354–2366. http://dx.doi.org/10.1029/2002EO000342.
Nozaki, Y., Zhang, J., Amakawa, H., 1997. The fractionation between Y and Ho in the marine environment. Earth Planet. Sci. Lett. 148, 329–340. http://dx.doi.org/10.1016/S0012-821X(97)00034-4.
Núñez-Useche, F., Barragan, R., 2012. Microfacies analysis and paleoenvironmental dynamic of the Barremian-Albian interval in Sierra del Rosario, eastern Durango state. Mexico. Rev. Mex. Ciencias Geol. 29, 204–218.
Núñez-Useche, F., Barragán, R., Canet, C., López-Martínez, R., 2016. Record of upper Aptian-lower Albian environmental perturbation in northeastern Mexico. J. S. Am. Earth Sci. 70, 298–307. http://dx.doi.org/10.1016/j.jsames.2016.05.011.
Ojeda, H.A.O., 1982. Structural framework, stratigraphy, and evolution of Brazilian marginal basins. Am. Assoc. Pet. Geol. Bull. 66, 732–749. http://dx.doi.org/10.1306/03B5A309-16D1-11D7-8645000102C1865D.
Pattan, J.N., Pearce, N.J.G., Mislankar, P.G., 2005. Constraints in using Cerium-anomaly of bulk sediments as an indicator of paleo bottom water redox environment: a case study from the Central Indian Ocean Basin. Chem. Geol. 221, 260–278. http://dx.doi.org/10.1016/j.chemgeo.2005.06.009.
Paula-Santos, G.M., Caetano-Filho, S., Babinski, M., Trindade, R.I., Guacaneme, C., 2017. Tracking connection and restriction of West Gondwana São Francisco Basin through isotope chemostratigraphy. Gondwana Res. 42, 280–305. http://dx.doi.org/10.1016/j.gr.2016.10.012.
Piper, D.Z., 1974a. Rare earth elements in the sedimentary cycle: a summary. Chem. Geol. 14, 285–304.
Piper, D.Z., 1974b. Rare earth elements in ferromanganese nodules and other marine phases. Geochim. Cosmochim. Acta 38, 1007–1022. http://dx.doi.org/10.1016/0016-7037(74)90002-7.
Piper, D.Z., Bau, M., 2013. Normalized rare earth elements in water, sediments, and wine: identifying sources and environmental redox conditions. Am. J. Anal. Chem. 4, 69–83. http://dx.doi.org/10.4236/ajac.2013.410A1009.
Ponte, F.C., Asmus, H.E., 2004. As bacias marginais brasileiras: estágio atual de conhecimento. Bol. Geociências da Petrobras 12, 385–420.
Premoli-Silva, I., Mcnulty, C.L., 1984. Planktonic foraminifers and calpionellids from Gulf of Mexico sites, Deep Sea Drilling Project leg 77. In: Buffler, R.T., Schlager, W. (Eds.), Initial Reports of DSDP 77. U.S. Government Printing Office, Washington, USA, pp. 547–584.
Ryan, W.B.F., Cita, M.B., 1977. Ignorance concerning episodes of ocean-wide stagnation. Mar. Geol. 23, 197–215. http://dx.doi.org/10.1016/S0070-4571(08)70558-2.
Sabatino, N., Coccioni, R., Salvagio Manta, D., Baudin, F., Vallefuoco, M., Traina, A., Sprovieri, M., 2015. High-resolution chemostratigraphy of the late Aptian-early Albian oceanic anoxic event (OAE 1b) from the Poggio le Guaine section (Umbria-Marche Basin, central Italy). Palaeogeogr. Palaeoclimatol. Palaeoecol. 426, 319–333. http://dx.doi.org/10.1016/j.palaeo.2015.03.009.
Santos, R.V., Alvarenga, C.J.S., Dardenne, M.A., Sial, A.N., Ferreira, V.P., 2000. Carbon and oxygen isotope profiles across Meso-Neoproterozoic limestones from central Brazil: Bambuí and Paranoá Groups. Precambrian Res. 104, 107–122.
Schijf, J., De Baar, H.J.W., Wijbrans, J.R., Landing, W.M., 1991. Dissolved rare earth elements in the Black Sea. Deep-Sea Res. 38, S805–S823.
Seilacher, A., Buatois, L.A., Mángano, M.G., 2005. Trace fossils in the Ediacaran-Cambriam transition: behavioral diversification, ecological turnover and environmental shift. Palaeogeogr. Palaeoclimatol. Palaeoecol. 227, 323–356. http://dx.doi.org/10.1016/j.palaeo.2005.06.003.
Shields, G., Stille, P., 2001. Diagenetic constraints on the use of cerium anomalies as palaeoseawater redox proxies: an isotopic and REE study of Cambrian phosphorites. Chem. Geol. 175, 29–48. http://dx.doi.org/10.1016/S0009-2541(00)00362-4.
Sholkovitz, E.R., Landing, W.M., Lewis, B.L., 1994. Ocean particle chemistry: the fractionation of rare earth elements between suspended particles and seawater. Geochim. Cosmochim. Acta 58 (6), 1567–1579.
Spadini, A.R., Esteves, F.R., Dias-Brito, D., Azevedo, R.L.M., Rodrigues, R., 1988. The Macaé Formation, Campos Basin, Brazil: its evolution in the context of the initial history of the South Atlantic. Rev. Bras. Geosci. 18 (3), 261–272.
Tachikawa, K., Jeandel, C., Vangriesheim, A., Dupr??, B., 1999. Distribution of rare earth elements and neodymium isotopes in suspended particles of the tropical Atlantic Ocean (EUMELI site). Deep-Sea Res. I Oceanogr. Res. Pap. 46, 733–755. http://dx.doi.org/10.1016/S0967-0637(98)00089-2.
Tedeschi, L.R., Jenkyns, H.C., Robinson, S.A., Sanjinés, A.E.S., Viviers, M.C., Quintaes, C.M.S.P., Vazquez, J.C., 2017. New age constraints on Aptian evaporites and carbonates from the South Atlantic: implications for Oceanic Anoxic Event 1a. Geology 45 (6), 543–546. http://dx.doi.org/10.1130/G38886.1.
Vincent, B., van Buchem, F.S.P., Bulot, L.G., Immenhauser, A., Caron, M., Baghbani, D., Huc, A.Y., 2010. Carbon-isotope stratigraphy, biostratigraphy and organic matter distribution in the Aptian – lower Albian successions of southwest Iran (Dariyan and Kazhdumi formations). Geoarabia Spec. Publ. 4 (1), 139–197.
Wang, Y.L., Liu, Y.G., Schmitt, R.A., 1986. Rare earth element geochemistry of South Atlantic deep sea sediments: Ce anomaly change at −54 My. Geochim. Cosmochim. Acta 50, 1337–1355. http://dx.doi.org/10.1016/0016-7037(86)90310-8.
Wang, Q., Lin, Z., Chen, D., 2014. Geochemical constraints on the origin of Doushantuo cap carbonates in the Yangtze Gorges area, South China. Sediment. Geol. 304, 59–70. http://dx.doi.org/10.1016/j.sedgeo.2014.02.006.
Webb, G.E., Kamber, B.S., 2000. Rare earth elements in Holocene reefal microbialites: a new shallow seawater proxy. Geochim. Cosmochim. Acta 64, 1557–1565.
Winter, W.R., Jahnert, R.J., França, A.B., 2007. Bacia de Campos. Bacias Sedimentares Bras. – Cart. Estratigráficas. 511–529.
Zhang, J., Nozaki, Y., 1996. Rare earth elements and yttrium in seawater: ICP-MS determinations in the East Caroline, Coral Sea, and South Fiji basins of the western South Pacific Ocean. Geochim. Cosmochim. Acta 60, 4631–4644. http://dx.doi.org/10.1016/S0016-7037(96)00276-1.
Zhang, J., Nozaki, Y., 1998. Behavior of rare earth elements in seawater at the ocean margin: a study along the slopes of the Sagami and Nankai troughs near Japan. Geochim. Cosmochim. Acta 62, 1307–1317. http://dx.doi.org/10.1016/S0016-7037(98)00073-8.
Zhang, J., Amakawa, H., Nozaki, Y., 1994. The comparative behaviors of Yttrium and Lanthanides in the seawater of the North Pacific. Geophys. Res. Lett. 21, 2677–2680.
Zhao, H., Jones, B., 2013. Distribution and interpretation of rare earth elements and yttrium in Cenozoic dolostones and limestones on Cayman Brac, British West Indies. Sediment. Geol. 284–285, 26–38. http://dx.doi.org/10.1016/j.sedgeo.2012.10.009.
Zhao, Y.Y., Zheng, Y.F., Chen, F., 2009. Trace element and strontium isotope constraints on sedimentary environment of Ediacaran carbonates in southern Anhui, South China. Chem. Geol. 265, 345–362. http://dx.doi.org/10.1016/j.chemgeo.2009.04.015.